Viral manipulation of mechanoresponsive signaling disassembles processing bodies

Elizabeth L. Castle[1], Carolyn-Ann Robinson[2], Pauline Douglas[3, 5], Kristina D. Rinker[3, 4, 5], and Jennifer A. Corcoran[1, 2, 5, 6]

[1]Department of Microbiology and Immunology, Dalhousie University, Halifax, NS, Canada
[2]Current address, Microbiology, Immunology and Infectious Diseases Department and Charbonneau Cancer Research Institute, University of Calgary, Calgary, AB, Canada.
[3]Department of Physiology and Pharmacology, University of Calgary, Calgary, AB, Canada.
[4]Department of Chemical and Petroleum Engineering and Centre for Bioengineering Research and Education, University of Calgary, Calgary, AB, Canada.
[5]Charbonneau Cancer Institute, University of Calgary, Calgary, AB, Canada.
[6]Corresponding Author

Abstract

Processing bodies (PBs) are ribonucleoprotein granules that suppress cytokine mRNA translation that are targeted for disassembly by many viruses. Kaposi's sarcoma-associated herpesvirus is the etiological agent of the inflammatory endothelial cancer, Kaposi's sarcoma, and a PB-regulating virus. The virus encodes Kaposin B (KapB), which induces actin stress fibres (SFs) and cell spindling as well as PB disassembly. We now show that KapB-mediated PB disassembly requires actin rearrangements, RhoA effectors and the mechanoresponsive transcription activator, YAP. Moreover, ectopic expression of active YAP or exposure of ECs to mechanical forces caused PB disassembly in the absence of KapB and mechanoresponsive PB disassembly also required YAP. Using the viral protein KapB, we identified a new consequence of the exposure of cells to mechanical forces that alter actin dynamics and activate YAP, namely the disassembly of PBs.

Importance

For the first time, we demonstrate that processing bodies (PBs), cytoplasmic sites of RNA decay, are regulated by mechanical signaling events that alter actin dynamics and that this requires the mechanoresponsive transcription factor, YAP. Using the overexpression of a viral protein called KapB, known previously to mediate PB disassembly, we show that actin stress fibers (SFs) and the mechanoresponsive transcription factor, YAP, are required for PB loss. We also show that other established mechanical signals (shear stress or stiff extracellular matrix) that lead to the formation of SFs and activate YAP also cause PB disassembly. This is important because it means that KapB activates, from the inside out, a pathway that links cell shape to post-transcriptional gene regulation via cytoplasmic PBs.

Introduction

Cells are exposed to a variety of environments and they respond to changes in external force by adjusting internal tension. These mechanical cues can be transmitted to the cell through changes to extracellular contact nodes (focal adhesions) and contractile actomyosin structures to maintain tension homeostasis (Friedland, Lee, and Boettiger 2009; Kong et al. 2009; del Rio et al. 2009; Grashoff et al. 2010; reviewed in Finch-Edmondson and Sudol 2016). Actin stress fibres (SFs) are cytoskeletal structures composed of thick actin bundles, often associated with focal adhesions (Vallenius 2013), that are force-responsive, maintaining cytoskeletal integrity in changing mechanical environments (Burridge and Guilluy 2016). SF formation is coordinated by the GTPase, RhoA; it activates the formin, mammalian diaphanous protein-1 (mDia1) to promote actin filament growth and Rho-associated coiled-coil kinase (ROCK) to promote actomyosin contractility through non-muscle myosin II (Watanabe et al. 1997; Amano et al. 1997; Kimura et al. 1996). These RhoA-effectors act together to promote the formation of contractile and stable actin filaments in response to mechanical and chemical stimuli (Watanabe et al. 1999).

External forces elicit a cascade of signals using actin as force transducers to alter gene expression. The activity of the mechanoresponsive transcriptional coactivator, Yes-associated protein (YAP), is controlled by cell shape and cytoskeletal structure (Dupont et al. 2011; Wada et al. 2011; Halder, Dupont, and Piccolo 2012; Yu et al. 2012). YAP is nuclear and active in response to low cell-cell contact (Zhao et al. 2007), high stiffness of the extracellular matrix (ECM) (Dupont et al. 2011), in shear stress due to fluid flow (K.-C. Wang et al. 2016; Nakajima et al. 2017; Lai and Stainier 2017; H. J. Lee et al. 2017; Huang et al. 2016), or after G-protein coupled receptor (GPCR) activation (Yu et al. 2012). Most of these signals induce the activity of RhoA and promote the formation of SFs, and studies have implicated actin cytoskeletal structures as requisite intermediates for YAP activation (Noria et al. 2004; Lee and Kumar 2016).

Nuclear YAP associates with its coactivators to mediate transcription of genes involved in cell proliferation, differentiation, survival and migration (Halder, Dupont, and Piccolo 2012). Consistent with this, nuclear YAP is often pro-tumourigenic and drives progression of many oncogenic traits in a variety of cancers. These include the induction of cell stemness (Panciera et al. 2016), altered metabolism (C. Yang et al. 2018), cancer cell invasion/vascular remodeling

56 (Calvo et al. 2013; Liu et al. 2018; Kimura et al. 2020), and altered growth and proliferation
57 (Kapoor et al. 2014; Zanconato et al. 2015; Jang et al. 2017).
58 Kaposi's sarcoma (KS) is an endothelial cell (EC) cancer that is caused by the virus,
59 Kaposi's sarcoma-associated herpesvirus (KSHV) (Chang et al. 1994; Russo et al. 1996; Zhong
60 et al. 1996; Ganem 1997). KSHV establishes persistent, life-long infection of its human host, and
61 displays two types of infection, latent and lytic. In KS, the majority of the tumour ECs are
62 latently infected while lytic replication is rare; in part, because these cells die as a result of viral
63 replication (Boshoff et al. 1995; Staskus et al. 1997; Umbach et al. 2010; Speck and Ganem
64 2010). KS tumour ECs elongate into a 'spindled' morphology and expel proinflammatory
65 cytokines and angiogenic factors, which promote tumour progression and create a highly
66 inflammatory tumour microenvironment. Many features of *in vivo* KS are recapitulated by *in*
67 *vitro* latent infection of primary ECs, or ectopic expression of individual KSHV latent genes,
68 including spindling and pro-inflammatory characteristics (Ensoli 1998; Ciufo et al. 2001;
69 Naranatt et al. 2003; Grossmann et al. 2006; Ojala and Schulz 2014; DiMaio et al. 2011). Both
70 spindling and proinflammatory gene expression can induced by two different KSHV latent
71 genes, vFLIP (Grossmann et al. 2006) and Kaposin B (KapB; (Corcoran, Johnston, and
72 McCormick 2015)), suggesting a linkage between these two phenotypes. Furthermore, during
73 their short lifetime, lytically infected cells also secrete large quantities of pro-inflammatory and
74 angiogenic molecules. A contributor to this secretory phenotype is the constitutively active viral
75 G protein-coupled receptor (vGPCR), a lytic viral protein that also promotes cell elongation,
76 RhoA activation and cytoskeletal remodeling (Shepard et al. 2001; Montaner et al. 2006;
77 Corcoran et al. 2012). vGPCR also activates YAP during KSHV lytic infection (Liu et al. 2015);
78 however, no information exists to demonstrate YAP involvement in KSHV latency.
79 One way that KSHV latency promotes the pro-inflammatory and pro-tumourigenic KS
80 microenvironment is via KapB-mediated disassembly of cytoplasmic ribonucleoprotein granules
81 called processing bodies (PBs) (Corcoran, Johnston, and McCormick 2015). PBs are involved in
82 many RNA regulatory processes such as RNA silencing, nonsense-mediated decay and mRNA
83 decay and translational suppression of mRNA (Eulalio, Behm-Ansmant, and Izaurralde 2007,
84 Horvathova et al. 2017, Tutucci et al. 2018, Wilbertz et al. 2019, Hubstenberger et al. 2017). We
85 and others have shown that PBs are the major site for the translational suppression or constitutive
86 decay of human mRNAs that code for potent regulatory molecules such as proinflammatory

87 cytokines (Franks and Lykke-Andersen 2007; Corcoran, Johnston, and McCormick 2015; Vindry
88 et al. 2017; Blanco et al. 2014). There are ~4500 of these transcripts, all of which bear
89 destabilizing AU-rich elements (AREs) in their 3'-untranslated regions (3'-UTRs) (Shaw and
90 Kamen 1986; Shyu, Greenberg, and Belasco 1989; Chen and Shyu 1995; Winzen et al. 1999;
91 Stoecklin, Mayo, and Anderson 2006; Franks and Lykke-Andersen 2007; Bakheet, Williams,
92 and Khabar 2006; Bakheet, Hitti, and Khabar 2017). PB abundance and composition is
93 extremely dynamic and responds to cellular stress (Sheth 2003; Kedersha and Anderson 2007;
94 Aizer et al. 2008; Takahashi et al. 2011). Specifically, activation of the stress-responsive
95 p38/MK2 MAP kinase pathway by KapB elicits PB disassembly and prevents constitutive ARE-
96 mRNA turnover or translation suppression (Winzen et al. 1999; Docena et al. 2010; Corcoran et
97 al. 2012; Corcoran and McCormick 2015; Corcoran, Johnston, and McCormick 2015). This is an
98 important yet underappreciated regulatory mechanism that fine tunes the production of potent
99 proinflammatory cytokines and angiogenic factors in KS.
100 Though PBs are dynamic and stress-responsive, the precise signaling events that lead to
101 PB assembly or disassembly are not well understood. We showed previously that KapB binds
102 and activates MK2, which then phosphorylates hsp27, complexes with p115RhoGEF, and
103 activates RhoA to elicit PB disassembly (Corcoran, Johnston, and McCormick 2015; Garcia et
104 al. 2009; McCormick and Ganem 2005). While it is well-established that RhoA coordinates SF
105 formation (Ridley and Hall 1992; Watanabe et al. 1999; Schmitz et al. 2000; Hotulainen and
106 Lappalainen 2006), the precise mechanism of how RhoA promotes PB disassembly is not
107 appreciated (Corcoran, Johnston, and McCormick 2015; Takahashi et al. 2011). In an effort to
108 better understand the regulation of PB disassembly by KapB and RhoA, we began by targeting
109 downstream RhoA effectors reported to promote SF formation to determine if the proteins
110 known to mediate cytoskeletal remodeling were also necessary for PB disassembly. We reasoned
111 that at some point we would be able to uncouple the signaling events that led to SFs from those
112 that led to PB disassembly. We were not. We now present data that conclusively shows KapB-
113 mediated PB disassembly is dependent not only on RhoA, but on cytoskeletal structures,
114 actomyosin contractility and the presence of the mechanoresponsive transcription transactivator,
115 YAP. We also present the first evidence of the involvement of YAP in the tumourigenic
116 phenotypes induced by a KSHV latent gene, KapB. We also extend these studies beyond their
117 impact on viral tumourigenesis, by determining the mechanical regulation of PB dynamics in the

118 absence of KapB expression, and show that induced cell contractility, cytoskeletal structures and
119 active YAP cause PB disassembly. Using a viral protein from an oncogenic virus, we have
120 discovered a mechanoresponsive signaling pathway that transduces signals from cell shape and
121 cytoskeletal structures to YAP to control PBs, post-transcriptional regulators of cellular gene
122 expression.
123
124 **Results**
125 **RhoA effectors controlling SF formation are required for PB disassembly**
126 We previously showed that KapB-mediated PB disassembly required RhoA (Corcoran,
127 Johnston, and McCormick 2015). In this work, we investigated whether downstream RhoA
128 effectors known to control SF formation also control PB disassembly. Mammalian diaphanous
129 protein 1 (mDia1) and Rho-associated coiled-coil kinase (ROCK) are considered the main
130 coordinators of RhoA-mediated SF formation (Watanabe et al. 1999; Tojkander, Gateva, and
131 Lappalainen 2012). mDia1 is a formin that promotes actin filament polymerization (Watanabe et
132 al. 1999). To examine whether mDia1 was required for KapB-mediated PB disassembly, we
133 designed short hairpin RNAs (shRNAs) to silence mDia1 mRNA. KapB- and vector- expressing
134 human umbilical vein endothelial cells (HUVECs) were transduced with mDia1-targeting
135 shRNAs and selected. Silencing efficacy was confirmed with immunoblotting (Fig 1A). PB
136 analysis was performed using CellProfiler to quantify immunofluorescence images stained for
137 the hallmark PB-resident protein, Enhancer of mRNA decapping 4 (EDC4), as described in
138 detail in the methods (J. H. Yu et al. 2005; Kedersha et al. 2008). Knockdown of mDia1
139 increased PBs in KapB-expressing cells (Fig 1B, D). mDia1-sh1 showed a greater increase in
140 PBs in comparison to mDia1-sh2 (Fig 1B), and also increased PBs in vector control cells, likely
141 because mDia1-sh1 reduced protein expression by 90% whereas mDia1-sh2 reduced it by 40-
142 50% (Fig 1A). To separate how silencing of mDia1 impacted baseline turnover of PBs from how
143 silencing impacts KapB-mediated PB disassembly, we calculated the ratio of PBs per cell in
144 KapB-expressing cells and normalized to PBs per cell in the control. This is important because
145 this calculation shows whether KapB is still able to disassemble PBs, relative to vector, in the
146 context of mDia1 silencing. If the ratio is ≥1 after sh-mDia1 treatment, it indicates that KapB is
147 no longer able to disassemble PBs in comparison to the vector control, and that mDia1
148 contributes directly to KapB-mediated PB disassembly. Conversely, if the ratio is ~ 0.4 to 0.6, it

149 indicates that KapB can still disassemble PBs even in the context of sh-mDia1 treatment. In this
150 case, we determined that silencing using both mDia1-sh1 and mDia1-sh2 restored the PB ratio in
151 KapB:Vector cells to ~1, indicating that the ability of KapB to disassemble PBs is lost after
152 mDia1 silencing and that this is a KapB-specific effect (Fig 1C). We note that this ratio will be
153 reported in subsequent figures for every RNA silencing or drug treatment applied to test KapB-
154 mediated PB disassembly. We also observed that mDia1 silencing did not eliminate SF
155 formation (Fig 1D) but, instead, increased elongated cells with visible actin SFs across the cell in
156 both vector and KapB conditions. The visible actin structures may represent different SF
157 subtypes or actin bundles that compensate for the loss of mDia1 (Hotulainen and Lappalainen
158 2006).
159 ROCK promotes SF formation by increasing actin contractility and inhibiting actin severing
160 activity (Julian and Olson 2014). Chemical inhibition of both isoforms of ROCK, ROCK1 and
161 ROCK2, with Y-27632 (Ishizaki et al. 2000) restored PBs in KapB-expressing cells and
162 increased the ratio of KapB:Vector PBs (Fig 2A-C). HUVECs treated with Y-27632 had
163 scalloped cell edges with minimal actin structure (Fig 2A). Y-27632 did not visibly alter cell
164 viability during the indicated treatment. To determine whether PB disassembly is dependent on a
165 single ROCK isoform, both ROCK1 and ROCK2 were knocked down with isoform-specific
166 shRNAs. Knockdown efficacy was confirmed with immunoblotting (Fig S1). Independent
167 knockdown of ROCK1 and 2 increased PBs counts in KapB-expressing cells (Fig 2D, F) and
168 restored the ratio of KapB:Vector PBs counts (Fig 2E). This indicated that both ROCK1 and
169 ROCK2 can contribute to KapB-mediated PB disassembly. ROCK2 knockdown showed more
170 robust PB restoration, both in terms of PB counts and PB size, than that seen with ROCK1
171 knockdown (Fig 2D, F). Quantification of PB counts in control cells for both pan-ROCK
172 inhibition and ROCK knockdown experiments is reported in Figure S1. While pan-ROCK
173 inhibition and ROCK1 knockdown treatments both eliminate SFs, ROCK2 knockdown retains
174 pronounced actin fibres in the cells (Fig 2F). Similar to mDia1 knockdown, this may indicate a
175 compensatory mechanism to retain cell shape and suggests that only a subset of SFs may be
176 required for PB disassembly. Taken together, these data show that inhibition of RhoA effectors
177 that mediate SF formation can reverse KapB-mediated PB disassembly. Put another way, we
178 have been unable to uncouple KapB-mediated inducement of SFs from KapB-mediated PB
179 disassembly.

180 ROCK phosphorylates and activates LimK, which then phosphorylates and inactivates
181 cofilin, an actin-severing protein (Ohashi et al. 2000). In this way, ROCK promotes SF formation
182 by inactivating cofilin. To investigate the role of cofilin in KapB-mediated PB disassembly,
183 shRNAs to knockdown cofilin expression were used (Fig S2). Since ROCK activation results in
184 less cofilin activity and reduced actin severing, we hypothesized that knockdown of cofilin in
185 KapB-expressing cells would augment KapB-mediated PB disassembly. Knockdown of cofilin
186 resulted in elongated cells with more SFs in both control and KapB-expressing cells (Fig S2).
187 Cofilin knockdown also induced PB disassembly in control cells and aided PBs disassembly in
188 KapB-expressing cells (Fig S2 B, C). This indicates that inhibition of cofilin elicits PB
189 disassembly and supports the hypothesis that reducing cofilin activity is one of the reasons that
190 KapB promotes SF formation and PB disassembly.
191
192 **Changes in cytoskeletal contractility control PB disassembly**
193 One of the downstream activities of the kinase, ROCK, is to phosphorylate myosin light
194 chain to induce non-muscle myosin II (NMII)-mediated actomyosin contraction (Mutsuki
195 Amano et al. 1996). Since ROCK is required for KapB-mediated PB disassembly, we
196 determined whether functional actomyosin contractility is also required. KapB-expressing cells
197 were treated with blebbistatin, which inhibits NMII-mediated actomyosin contractility by
198 maintaining NMII in a conformation that is unable to bind actin filaments (Kovacs et al. 2004).
199 Treatment of KapB-expressing cells with blebbistatin restored both PBs levels in KapB-
200 expressing cells, as well as the KapB:Vector ratio of PBs (Fig 3A-C), indicating that
201 contractility is required for KapB-induced PB disassembly. ECs treated with blebbistatin had
202 normal actin structure (Fig 3C). Blebbistatin treatment for the indicated time did not visibly
203 alter cell viability. To determine if contraction would elicit the same phenotype in the absence
204 of KapB, cells were treated with Calyculin A (CalA), an inhibitor of myosin light chain
205 phosphatase that promotes NMII phosphorylation and actomyosin contraction (Asano and
206 Mabuchi 2001). CalA treatment did not visibly alter actin cytoskeletal structure or cell viability.
207 Inducing contraction with CalA decreased counts of PBs (Fig 3D, E), again consistent with the
208 hypothesis that actomyosin contractility controls PB disassembly. Actomyosin contractility
209 impacts cytoskeletal tension in adherent cells with SFs (Katoh et al. 1998; Tan et al. 2003).
210 Since the mechanoresponsive transcription activator, YAP, is activated by increases to

211 cytoskeletal tension via actomyosin contractility (Dupont et al. 2011), we explored the role of
212 YAP in KapB-mediated PB disassembly.
213
214 **YAP is required for KapB-mediated PB disassembly**
215 To determine if YAP was involved in KapB-mediated PB disassembly, we expressed
216 shRNAs targeting YAP in KapB-expressing HUVECs to assess whether the altered levels of
217 YAP impacted PB disassembly. Immunoblotting confirmed knockdown efficiency of YAP (Fig
218 4A). Knockdown of YAP resulted in elongated HUVECs with mostly cortical actin fibres (Fig
219 4D). These cells displayed increased PBs in KapB-expressing cells (Fig 4B-D). In the context of
220 YAP knockdown, the KapB:Vector ratio of PBs counts was restored, indicating that YAP is
221 required for KapB-mediated PB disassembly (Fig 4C) and suggesting that KapB is activating a
222 mechanoresponsive signalling axis to elicit PB disassembly via YAP.
223 We next investigated the steady-state protein level and localization of YAP in KapB-
224 expressing cells. KapB-transduced HUVECs showed increased levels of nuclear YAP and total
225 YAP in some experiments, though the ratio of nuclear:cytoplasmic YAP was not markedly
226 increased (Fig S3A-B). When YAP is phosphorylated by LATS, most notably at serine 127, it is
227 sequestered in the cytoplasm and transcriptionally inactive (Zhao et al. 2007). To investigate the
228 phosphorylation status of YAP in KapB-expressing cells, levels of P(S127)-YAP and total YAP
229 were measured by immunoblot. In KapB-expressing cells, there was a decrease in the ratio of
230 P(S127)-YAP to total YAP that may suggest YAP is more active when KapB is expressed (Fig
231 S3B). In some experiments, we observed an increase in total steady-state levels of YAP by
232 immunoblotting, corroborating the small increase in total YAP intensity seen by microscopy (Fig
233 S3A-B). Although increased total YAP may suggest that YAP turnover is blocked by KapB,
234 these increases were not accompanied by a strong decrease in phosphorylated YAP or an
235 increase in nuclear YAP, as in (Pavel et al. 2018).
236 We next asked if active YAP can interact with TEAD and other transcription factors to
237 elicit changes in gene expression in KapB-expressing cells (Vassilev et al. 2001). We used YAP
238 5SA, a constitutively active version of YAP that is unable to be phosphorylated and inactivated
239 by the inhibitory kinase LATS, as a positive control (Zhao et al. 2007). KapB did not increase
240 steady-state mRNA levels of common YAP target genes CTGF, CYR61 and ANKRD1 by RT-
241 qPCR, although these genes were elevated by YAP 5SA (Fig S3C). These data indicate despite

242 the observation that YAP may be more abundant in KapB-expressing cells, canonical YAP
243 targets are not upregulated. We wondered if YAP activation could elicit PB disassembly in the
244 absence of KapB expression. To this end, we transduced HUVECs with constitutively active
245 YAP 5SA. YAP 5SA-expressing cells contained few, thick actin fibres (Fig 5A) and displayed
246 decreased number of PBs per cell, indicating that YAP 5SA elicited disassembly of PBs (Fig 5A,
247 B). We also confirmed that we could stain PBs in control cells with antibodies for more than one
248 PB resident protein (EDC4, Dcp1a and DDX6) and that when YAP 5SA was expressed, loss of
249 PB puncta was observed for each of these staining conditions (Fig 5 A-E). Although PB
250 disassembly is induced by the expression of both YAP 5SA and KapB, active YAP increases the
251 transcriptional activation of genes CTGF, CYR61 and ANKRD1 while KapB does not.
252 We wondered if PB disassembly did depend on the ability of YAP to transactivate
253 transcription of its canonical genes. To better understand this, we transduced HUVECs with
254 another YAP construct called YAP 6SA (Fig 6). YAP 6SA contains the same mutations as 5SA;
255 in addition, it cannot be phosphorylated by AMPK at serine 94 (Mo et al. 2015). This
256 phosphorylation event is essential for its interaction with TEAD; therefore, the S94A mutation
257 renders YAP 6SA transcriptionally inactive (Mo et al. 2015, Zhang et al. 2017). We observed
258 that unlike YAP 5SA or KapB, YAP 6SA did not appear to elongate cells, suggesting that actin
259 dynamics were unaffected, as in Pavel et al. (2018). Compared to YAP 5SA which caused
260 pronounced PB disassembly, YAP 6SA failed to alter PB levels compared to vector controls (Fig
261 6B). This was confirmed by staining PBs with antibodies for two different resident proteins,
262 DDX6 and EDC4 (Fig 6A).
263
264 **YAP activators disassemble PBs**
265 Since overexpression of constitutively active YAP 5SA leads to disassembly of PBs, we
266 wanted to determine whether other stimuli that activated endogenous YAP could do the same.
267 We tested various upstream mechanical signals described to activate YAP for their ability to
268 elicit PB disassembly: shear stress, low cell confluence and high ECM stiffness (Nakajima et al.
269 2017; Lee et al. 2017; Noria et al. 2004; Zhao et al. 2007; Dupont et al. 2011). For the first, we
270 subjected HUVECs to shear stress by fluid flow (shear forces of 2 and 10 dyn/cm^2) and PBs were
271 examined via immunofluorescence using antibodies to both EDC4 and DDX6. Both treatments
272 showed prominent cell elongation, stress fibre formation, and resulted in robust PB disassembly

273 of both EDC4-positive and DDX6-positive puncta (Fig 7A, B). To test if cell confluence
274 regulates PB levels, HUVECs were seeded at low, medium and high densities. Cells at low
275 confluence are reported to have active YAP and we predicted PBs would disassemble; however,
276 the low-density monolayer displayed more PBs per cell then those at medium and high densities
277 (Fig 7C, D). To test the impact of collagen stiffness on PB disassembly, HUVECs were plated on
278 coverslips coated with increasing densities of collagen (0 to 64 μg/ cm^2). While collagen density
279 does not perfectly reproduce matrix stiffness as it does not differentiate the effect of matrix
280 stiffness from increasing collagen-binding sites, increasing collagen densities do correlate with
281 increased matrix stiffness (Yang, Leone, and Kaufman 2009; Lee et al. 2014; Joshi, Mahajan,
282 and Kothapalli 2018). As collagen density increased, PBs decreased (Fig 7E, F). Notably, as
283 collagen density increased, only slight increases in visible actin fibres were noted (Fig 7E),
284 suggesting the tested range of stiffness was small and should be expanded in future studies.
285 Taken together, these data indicate that PB disassembly occurred in response to mechanical
286 stimuli known to require RhoA and altered cytoskeletal structures to activate YAP (shear stress
287 and increased ECM concentration) (Zhao et al. 2012; Huang et al. 2016; Lee and Kumar 2016;
288 Moreno-Vicente et al. 2018) but not in response to YAP stimuli that do not also change actin
289 cytoskeletal structures (low cell confluence). These data support the importance of actin SF
290 formation and YAP activation as requisite precursors for PB disassembly not only YAP
291 activation status.
292
293 **Shear stress mediated PB disassembly requires YAP**
294 YAP responds to external forces that induce active RhoA, actin SFs, and pronounced cell
295 elongation; in short, the typical behaviour of ECs in response to the mechanical shear stress that
296 is produced by fluid flow. However, how YAP responds to shear stress is less clear (Wang et al.
297 2016; Huang et al. 2016; Lee et al. 2017; Nakajima and Mochizuki 2017). To verify YAP
298 activation by continuous, unidirectional fluid flow in our system, HUVECs subjected to 2 and 10
299 dyn/cm^2 of shear stress were lysed and used for immunoblotting for P(S127)-YAP and total
300 YAP. Shear stress decreased the ratio of phospho-YAP/YAP in both conditions, suggesting a
301 higher proportion of active YAP (Fig 8A). To assess if YAP was required for PB disassembly in
302 response to shear stress, HUVECs transduced with YAP-targeting shRNA were subjected to 10
303 dyn/cm^2 shear stress. PBs disassembled in cells treated with a non-targeting shRNA when

304 subjected to shear stress (Fig 8B, C), consistent with earlier experiments (Fig 7A, B). When YAP
305 was reduced by shRNA expression, ECs exposed to shear stress had more PBs than static growth
306 control cells (Fig 8B, C). YAP knockdown also reduced the cells ability to form SFs, with many
307 cells displaying highly cortical phalloidin staining and fewer actin fibres across the cell (Fig 8C).
308 Therefore, YAP is required to disassemble PBs after KapB is expressed and also in response to
309 shear stress.
310 Taken together with our analysis of KapB-mediated PB disassembly, these data suggest that
311 when KapB is expressed, it turns on mechanoresponsive signals that cells use to withstand
312 mechanical forces like shear, in the absence of an external stimulus. The outcome of both KapB
313 expression and exposure to mechanical forces is YAP-dependent disassembly of cytoplasmic
314 PBs (Fig 8D).
315
316 **Discussion**
317 In this manuscript, we have used a viral protein from an oncogenic virus to uncover a
318 new relationship between cytoplasmic PBs and the mechanical regulation of actin SF formation
319 and YAP. We present data to support the existence of a mechanoresponsive pathway that links
320 actin SFs, actomyosin contractility, and the transcription transactivator YAP to the disassembly
321 of PBs and show that this pathway is hijacked by KapB during KSHV latency. Our major
322 findings are as follows. i) KapB-mediated PB disassembly requires actin SF effectors ROCK1/2
323 /mDia1 and is enhanced by loss of the actin-severing protein, cofilin. ii) KapB-mediated PB
324 disassembly is reversed when blebbistatin is used to inhibit actomyosin contractility or after
325 knockdown of the mechanoresponsive transcription transactivator, YAP. iii) In the absence of
326 KapB, we can induce PB disassembly when we promote actomyosin contractility and YAP
327 activity using Calyculin A (inhibits myosin light chain phosphatase to promote actomyosin
328 contraction (Asano and Mabuchi 2001)), or overexpression of active YAP (YAP 5SA). Exposure
329 of endothelial cells to mechanical forces created by shear stress or a stiff extracellular matrix also
330 induces PB disassembly in the absence of KapB. iv) Overexpression of transcriptionally inactive
331 YAP (YAP 6SA) fails to disassemble PBs, indicating that YAP's role as a transcription
332 transactivator is important for its ability to promote PB disassembly. Together, these data show
333 for the first time, that PBs disassemble in response to mechanical signals that transduce external
334 forces from outside the cell to the actin cytoskeleton and that this pathway requires YAP.

335 Moreover, this work also highlights the remarkable pizzazz used by viruses to hijack cellular
336 pathways. In this case, we reveal that the viral protein KapB taps into this mechanoresponsive
337 pathway to trigger mechanical changes to cytoskeletal structures and downstream effectors like
338 YAP that would normally respond to force, thereby inducing PB disassembly from within the
339 cell, rather than from without.

340 Although SFs with periodic distribution of actin-crosslinking proteins and non-muscle
341 myosin II (NMII) have the potential to be contractile structures, in order to be able to generate
342 tension, SFs must be tethered at the ends (Katoh et al. 1998; Tan et al. 2003). Ventral SFs are
343 attached at both termini to the extracellular matrix (ECM) through focal adhesions and contain
344 NMII, which imparts a contractile phenotype, whereas dorsal SFs are attached through focal
345 adhesions but do not contain NMII, and thus are not contractile (Hotulainen and Lappalainen
346 2006; Small et al. 1998; Vallenius 2013). Several features of our data suggest that the actin
347 structures that are important for KapB-mediated PB disassembly must be contractile and cause
348 cytoskeletal tension. When both mDia1 and ROCK2 were silenced in KapB-expressing cells (Fig
349 1, 2), visible actin bundles are still apparent despite PB restoration in both contexts. This
350 suggests that not all SF subtypes are required for our phenotype. In addition, blebbistatin
351 treatment of KapB-expressing cells dramatically restored PBs; these data suggest that PB
352 disassembly requires actin-mediated contractility rather than structural support (Fig 3).
353 Furthermore, shear stress and increased ECM stiffness (Lee et al. 2006; Jackson et al. 2008) both
354 induced PB disassembly (Fig 7), reinforcing the correlation between increasing cell tension and
355 PB disassembly. Finally, our data show that YAP is required for PB disassembly (Figs 4, 5, 8).
356 YAP is mechanoresponsive; it becomes active when tension-forming actin structures are induced
357 by external forces e.g. focal adhesion engagement by stiff ECM (Dupont et al. 2011; Sugimoto et
358 al. 2018). As YAP activation and PB disassembly both rely on RhoA-induced cytoskeletal
359 contractility, any activator of YAP that induces cytoskeletal tension through RhoA should
360 mediate PB disassembly. Our data support this notion, as shear stress forces and increasing
361 collagen density both cause PB disassembly in the absence of KapB, while low confluence does
362 not (Fig 7). We also know that GPCRs ($G_{11/12}$ and $G_{q/}$11) activate YAP in a RhoA-dependent
363 manner (Yu et al. 2012) and LPA treatment or overexpression of KSHV-derived constitutively
364 active vGPCR (both activate $G_{11/12}$) both induce PB disassembly (Corcoran et al. 2012; Corcoran
365 and McCormick 2015). These findings support the conclusion that PB disassembly requires the

366 formation of contractile actin structures like those associated with YAP transactivation
367 responses.
368 Data presented herein clearly implicate a requirement for YAP in the PB disassembly
369 phenotype that is induced by KapB and by the external force imparted by shear stress (Fig 4, 8).
370 However, the precise connection between YAP and PB disassembly is unclear. Despite the clear
371 reliance on YAP for PB disassembly, KapB does not increase expression of canonical YAP-
372 regulated transcripts (Fig S3). Our data also show small increases in total YAP and small
373 decreases in the ratio of phosphorylated/total YAP; however, the ratio of nuclear:cytoplasmic
374 YAP is not markedly altered (Fig S3). Taken together, these data first suggested a model
375 whereby PB disassembly was independent of the role of YAP as a gene transactivator and YAP
376 nuclear translocation. However, we found that overexpression of YAP 6SA, which is unable to
377 act as a transcription transactivator, failed to cause PB disassembly (Fig 6), indicating that the
378 transcription induction function of YAP is required for its role in regulating PB dynamics. Future
379 experimentation is needed to further define the mechanistic link between YAP activation and PB
380 disassembly.
381 KSHV is an oncogenic virus associated with the endothelial neoplasm, Kaposi's sarcoma
382 (KS). Cells within the KS lesion display latent KSHV infection, proliferate abnormally, spindle,
383 and release many pro-inflammatory and pro-tumourigenic mediators into the microenvironment.
384 KapB expression is sufficient to recapitulate two of these key features, cell spindling and pro-
385 inflammatory mediator production that results from enhanced stability of ARE-containing
386 cytokine mRNAs that would normally shuttle to PBs for constitutive turnover (Corcoran,
387 Johnston, and McCormick 2015). Our previous work showed that both phenotypes utilize KapB
388 activation of the stress-responsive kinase, MK2, and the downstream activation of the GTPase
389 RhoA (Corcoran, Johnston, and McCormick 2015; Corcoran and McCormick 2015). We have
390 now extended these studies to show that PB disassembly depends on mechanical signals that
391 cause cell elongation, actin contractility and activate YAP. However, other KSHV gene products
392 have been observed to induce cell elongation and/or cytoskeletal changes. These include the
393 latent protein vFLIP, and two lytic proteins, vGPCR and the viral thymidine kinase (TK)
394 (Corcoran et al. 2012, Grossman et al. 2006; Gill et al. 2005; Gill et al. 2015; Lagunoff 2015;
395 Shepard et al. 2001). Both vFLIP and vGPCR cause cell elongation, while KSHV-TK causes
396 RhoA-dependent cell contraction that leads to cell detachment (Corcoran et al. 2012, Grossman

397 et al. 2006; Gill et al. 2015, Shepard et al. 2001). We previously showed that the lytic vGPCR
398 protein mediates PB disassembly and the concomitant stabilization of ARE-mRNAs, (Corcoran
399 et al. 2012); however, how vFLIP or KSHV-TK expression influences PB dynamics is unknown.
400 The observation that KSHV encodes multiple gene products that alter cytoskeletal dynamics and
401 promote inflammatory gene expression via PB disassembly further supports the linkage of these
402 two phenotypes during KSHV infection.
403 PBs are sites where innate immune factors congregate that are disrupted by most viruses
404 during infection (Burdick et al. 2010; Li et al. 2012; Ostareck, Naarmann-de Vries, and
405 Ostareck-Lederer 2014; Burgess and Mohr 2015; Cuevas et al. 2016; H. Wang et al. 2016; Lumb
406 et al. 2017; Balinsky et al. 2017; Núñez et al. 2018; Ng et al. 2020). KSHV encodes three
407 separate proteins that all induce PB disassembly, KapB, vGPCR and ORF57, suggesting this
408 event is central to viral persistence (Corcoran et al. 2012; Corcoran, Johnston, and McCormick
409 2015; Sharma et al. 2019). PBs are likely playing an as yet undefined and underappreciated role
410 in regulating innate antiviral responses. KSHV encodes two proteins that influence YAP activity,
411 suggesting YAP activation is also central to KSHV biology (Liu et al. 2015). YAP is an
412 unappreciated negative regulator of innate immune signaling pathways. YAP blocks the ability
413 of the innate immune kinase, TBK1, a downstream effector for several innate signaling
414 pathways, to associate and activate its substrates (Zhang et al 2017). In so doing, YAP blocks
415 downstream induction of interferons and increases viral replication (Zhang et al. 2017).
416 However, this feature of YAP is independent of its ability to act as a transcriptional
417 transactivator (Zhang et al. 2017). Based on our data that show YAP 5SA causes PB disassembly
418 while YAP 6SA does not, KapB-induced PB disassembly requires the transcription
419 transactivation function of YAP. We speculate that KapB-induced PB disassembly, like active
420 YAP, favours viral replication and survival and is promoted by KSHV in order to reshape
421 subsequent antiviral innate immune responses.
422 In this manuscript, we describe the surprising convergence of two previously unrelated
423 yet essential regulators of cellular gene expression – the mechanoresponsive transactivator YAP
424 and cytoplasmic PBs, known sites of AU-rich cytokine mRNA decay or translational
425 suppression. We show that PB disassembly is mechanoresponsive; external forces that change
426 cell shape and tension-forming cytoskeletal structures cause PB disassembly in a YAP-
427 dependent manner. This discovery was made courtesy of the unique KSHV protein, KapB, and

428 provides yet another example of how viruses have evolved surprising ways to manipulate their
429 host and ensure their survival. In this case, KapB induces, from the inside out, a
430 mechanoresponsive pathway to cause PB disassembly. Future study will untangle how these
431 related mechanoresponsive events are induced by KSHV to better promote viral replication.
432
433
434

435 **Materials and Methods**

436 **Antibodies, Plasmids and Reagents**

437 The antibodies used in this study can be found in Table S1. The plasmids used in this study
438 can be found in Table S2. Forward and reverse shRNA sequences were selected from the TRC
439 Library Database in the Broad Institute RNAi consortium. YAP target shRNAs in pLKO.1 were
440 obtained from Dr. C. McCormick (Dalhousie University, Halifax, Canada). Sequences for all
441 shRNA oligonucleotides used for cloning are listed in Table S3. Cloning of shRNAs was
442 conducted according to the pLKO.1 protocol (Addgene 2006). YAP 6SA was subcloned into
443 pLJM1 by PCR amplification using primers (For: 5'-CGTAACCGGTATGGATCCCGGGCA-
444 3', Rev: 5'-CTGATAAGTCGACAACCACTTTGTACAAGAAAGTTG-3') designed to remove
445 the V5 tag and insert a stop codon as well as 5' AgeI and 3' SalI restriction enzyme sites. The
446 chemical inhibitors used in this study can be found in Table S4.

447 **Cell Culture**

448 Human embryonic kidney 293T and 293A cells (HEK-293T/A, ATCC, Manassas,
449 Virginia, US) and human cervical adenocarcinoma cells expressing a tetracycline-inducible
450 repressor (HeLa Tet-Off, Clontech, Mountain View, California, US) were cultured in Dulbecco's
451 Modified Eagle Medium (DMEM, Gibco, Carlsbad, California, US) supplemented with 10%
452 heat-inactivated fetal bovine serum (Gibco), 100 U/mL penicillin, 100 μg/mL streptomycin, and
453 2 mM L-glutamine (Gibco). Pooled human umbilical vein endothelial cells (HUVECs, Lonza,
454 Basel, Switzerland) were cultured in endothelial cell growth medium 2 (EGM-2, Lonza)). For
455 HUVEC passaging, tissue culture plates were precoated for 30 min at 37˚C with 0.1% (w/v)
456 porcine gelatin (Sigma, St. Louis, Missouri, US) in 1X PBS (Gibco). All cells were routinely
457 tested for mycoplasma by PCR method.

458 **Transfection for Lentivirus Production**

459 HEK-293T cells at 70-80% confluence were transfected using 3.3 μg of the target lentiviral
460 construct, 2 μg pSPAX2 and 1 μg pMD2.G with 1 mg/mL polyethyenimine (PEI, Sigma) in
461 serum-free DMEM. After 5 to 6 h, media was replaced with antibiotic-free DMEM containing
462 10% FBS and 2 mM L-glutamine (Gibco). Transfected cells were incubated for 48 h at 37˚C to
463 allow lentivirus production. The supernatant media containing viral particles was harvested and
464 filtered through a 0.45 μm polyethersulfone (PES) filter (VWR, Randor, Pennsylvania, US) and
465 aliquoted. Virus was stored at -80˚C until use.

466 **Lentiviral Transduction**

467 Lentivirus was supplied to wells of plated HUVECs in EGM-2 supplemented with 5
468 μg/mL hexadimethrine bromide (polybrene). After 24 h incubation, cells were selected with
469 either 5 μg/mL blasticidin (Sigma) for 96 h, replacing the media and antibiotic at 48 h, or 1
470 μg/mL puromycin (Sigma) for 48 h. Following selection, HUVEC medium was replaced with
471 EGM-2 without selection for at least 24 h recovery before further use. Lentivirus was titrated to
472 ensure no significant changes in cell viability from non-targeting control.

473 **Immunofluorescence**

474 Immunofluorescence was performed as described previously (Corcoran, Johnston, and
475 McCormick 2015). Briefly, cells were grown on coverslips (no. 1.5, Electron Microscopy
476 Sciences, Hatfield, Pennsylvania, US). Following treatment, coverslips were fixed in 4%
477 paraformaldehyde (PFA, Electron Microscopy Sciences) in PBS at 37°C for 10 min,
478 permeabilized with 0.1% Triton-X100 (Sigma) in 1X PBS for 10 min at RT, and blocked in 1%
479 Human AB serum (blocking buffer, Sigma) in 1X PBS for 1 h at RT. Coverslips were then
480 incubated with diluted primary antibody in blocking buffer overnight at 4°C in a humidified
481 chamber. After primary antibody incubation, coverslips were washed with 1X PBS and then
482 incubated in fluorescently-tagged secondary antibody diluted in blocking buffer for 1 h at RT. If
483 applicable, coverslips were stained with Phalloidin-conjugated Alexa-Fluor 647 (Invitrogen,
484 1:100) in 1X PBS for 1.5 h. Coverslips were mounted onto microscope slides (FisherBrand,
485 Pittsburgh, Pennsylvania, US) using Prolong Gold Antifade Mounting Media (Invitrogen,
486 Carlsbad, California, US). For coverslips that were used for EDC4 puncta quantification, the
487 following modifications to immunofluorescence were made: (1) Prior to permeabilization,
488 coverslips were stained with wheat germ agglutinin (WGA) Alexa-647 conjugate (Invitrogen,
489 1:400) in 1X PBS for 10 min at RT. (2) Following secondary antibody incubation, coverslips
490 were stained with 4',6-Diamidino-2-Phenylindole (DAPI, Invitrogen, 1:10,000) in 1X PBS for 5
491 min.

492 Confocal imaging was performed on the Zeiss LSM 880 Confocal Microscope
493 (Charbonneau Microscopy Facility, University of Calgary, Calgary, Canada) at the 63X oil
494 objective. CellProfiler imaging was performed on the Zeiss AxioImager Z2 (CORES facility,
495 Dalhousie University, Halifax, Canada) or Zeiss AxioObserver (Charbonneau Microscopy
496 Facility, University of Calgary) at the 40X oil objective.

497 **Quantification of Processing Bodies Using CellProfiler Analysis**

498 CellProfiler (cellprofiler.org) is an open source software for high-content image analysis
499 (Kamentsky et al. 2011) and was used to develop an unbiased method for quantifying changes to
500 PB dynamics. The pipeline used for quantifying PBs was structured as follows: To detect nuclei,
501 the DAPI image was thresholded into a binary image. In the binary image, primary objects
502 between 30 to 200 pixels in diameter were detected and defined as nuclei. Cells were identified
503 as secondary objects in the WGA image using a propagation function from the identified nuclei,
504 which determined the cell's outer edge. Using the parameters of a defined nucleus and cell
505 border, the cytoplasm was then defined as a tertiary object. The EDC4 channel image was
506 enhanced using an "Enhance Speckles" function to identify distinct puncta and eliminate
507 background staining. The cytoplasm image was then applied as a mask to the enhanced puncta
508 image to ensure quantitation of only cytoplasmic puncta. EDC4 puncta were measured in the
509 cytoplasm of cells using a 'global thresholding with robust background adjustments' function as
510 defined by the program. The threshold cut-off for identified EDC4 puncta remained constant
511 between all experiments with identical staining parameters. Puncta number per cell, intensity and
512 locations with respect to the nucleus were measured and exported as .csv files and analyzed in
513 RStudio. A template of the RStudio analysis pipeline is attached in Appendix A. Data was
514 represented as fold change in EDC4 puncta count per cell normalized to the vector puncta count.
515 'Relative EDC4 Puncta/Cell (KapB/Vector)' demonstrates the KapB puncta count divided by
516 vector puncta count, a ratio that was calculated within each treatment group for each biological
517 replicate.

518 **Protein Electrophoresis and Immunoblotting**

519 Cells were lysed in 2X Laemmli buffer (20% glycerol, 4% SDS, 120 mM Tris-HCl),
520 between 150 to 300 μL, depending on cell density. Lysates were homogenized with a 0.21-gauge
521 needle, and supplemented to contain 0.02% (w/v) bromophenol blue (Sigma) and 0.05 M
522 dithiothreitol (DTT, Sigma), then heated at 95˚C for 5 min. 7.5 or 12% TGX Stain-Free SDS-
523 polyacrylamide gels (BioRad) were cast according to the instructions of the manufacturer and 5
524 to 15 μg of total protein were subjected to SDS gel electrophoresis using 1X SDS running buffer
525 (25 mM Tris, 192 mM Glycine, 0.1% SDS). Precision Plus Protein All Blue Prestained Protein
526 Standards (BioRad, Hercules, California, US) was used as a molecular weight marker. After
527 electrophoresis, gels were UV-activated using the ChemiDocTouch (BioRad) Stain-Free Gel

528 setting with automated exposure for 45 s. The protein was transferred to low-fluorescence
529 polyvinylidene difluoride (PVDF) membranes (BioRad) on the Trans-Blot Turbo Transfer
530 System (BioRad) according to the instructions of the manufacturer. Following transfer, total
531 protein amounts on membranes were imaged on the ChemiDocTouch using the Stain-Free
532 Membrane setting with automated exposure. Membranes were then blocked using 5% BSA
533 (Sigma) in 1X TBS-T (150 nM NaCl, 10 mM Tris, pH 7.8, 0.01% Tween-20) for 1 h at RT.
534 Primary antibody was diluted in 2.5% BSA in 1X TBS-T. Membranes were incubated in
535 primary antibody solution overnight at 4°C with rocking. The following day, membranes were
536 washed 3 times for 5 min in 1X TBS-T. Membranes were incubated with the appropriate
537 secondary antibody, conjugated to horseradish peroxidase (HRP) for 1 h at RT. Membranes were
538 washed 4 times for 5 min in 1X TBS-T. Clarity™ Western ECL Blotting Substrate (BioRad) was
539 mixed at a 1:1 ratio and applied to the membrane for 5 min. Chemiluminescent signal was
540 imaged on ChemiDocTouch Chemiluminescence setting. Band intensity was quantified using
541 ImageLab software (BioRad), normalizing to total protein.

542 **Quantitative Reverse-Transcriptase Polymerase Chain Reaction (qRT-PCR)**

543 Cells were lysed in 250 μL RLT buffer (Qiagen, Hilden, Germany) and RNA was
544 extracted using the RNeasy Plus Mini kit (Qiagen) according to the manufacturer's instructions.
545 Complementary DNA (cDNA) was synthesized from 1 μg of total RNA using the qScript cDNA
546 SuperMix (QuantaBio, Hilden, Germany) according to the manufacturer's instructions. Real-
547 time quantitative PCR with SsoFast EvaGreen qPCR MasterMix (BioRad) was used to quantify
548 the fold-change in mRNA abundance. Relative fluorescence was quantified using CFX Connect
549 (BioRad). All qRT-PCR primers efficiencies were between 90-110% in HUVECs and sequences
550 are found in Table S5.

551 **Collagen-Coating for Altering Matrix Stiffness**

552 Coverslips (no. 1.5, Electron Microscopy Sciences) were coated with a dilution series (0 to
553 64 μg/cm^2) of rat-tail collagen-1 (Gibco) in 0.02 M acetic acid for 4 h at RT. Slides were
554 sterilized with UV irradiation and washed with 2 times with sterile 1X PBS prior to seeding
555 cells.

556 **Unidirectional Fluid Flow for Endothelial Cell Shear Stress**

557 A parallel-plate flow chamber was used to expose ECs to shear stress. The system was
558 described in detail in Gomez-Garcia et al. (2018). Briefly, cleaned, unfrosted microscope slides

559 (Cole-Parmer, Vernon Hills, Illinois, US) were coated for 4 h at RT with rat-tail collagen-1
560 (Gibco) in 0.02 M acetic acid for a resultant 8.3 μg/cm^2 collagen density. Slides were sterilized
561 with UV irradiation and washed 2 times with sterile 1X PBS. HUVECs were seeded at a density
562 of 350,000 cells/slide and cultured for 24 h. Forty-five mL of EGM-2 supplemented with dextran
563 (Spectrum Chemical, New Brunswick, New Jersey, US) for a resultant 3 cP viscosity was added
564 to the stock media bottle. The stock media bottle was connected with the associated tubing and
565 pulse dampener. Slides with seeded cells were inserted onto the flow chamber, a gasket
566 (Specialty Manufacturing, Calgary, Canada) was added, and the system was sealed shut and
567 attached to the flow loop following the outlet of a pulse dampener. The rate of fluid flow was
568 started at 0.3 L/min and doubled every 15 min until final flow rates of 0.6 L/min and 2.7 L/min
569 were reached, corresponding to shear stress rates of 2 and 10 dyn/cm^2. Following 21 h, cells were
570 removed and immediately fixed for immunofluorescence or lysed for immunoblotting.

571 **Statistical Analysis**

572 Statistical analysis was performed in GraphPad Prism 8.0 software. Significance was
573 determined using a ratio paired t-test or repeated measures analysis of variance (ANOVA). One-
574 tailed ratio paired t-tests were applied in comparisons specifically examining PB restoration in
575 KapB-expressing cells as a directional hypothesis. In all other comparisons, two-tailed ratio
576 paired t-tests were applied. Significance was determined at $p = 0.05$. Each biological replicate
577 for CellProfiler quantification consisted of 6 images of each treatment in a given experiment,
578 counting approximately 100 to 200 cells per treatment.
579

580 **References**

581 Aizer, Adva, Yehuda Brody, Lian Wee Ler, Nahum Sonenberg, Robert H. Singer, and Yaron
582 Shav-Tal. 2008. "The Dynamics of Mammalian P Body Transport, Assembly, and
583 Disassembly In Vivo." *Molecular Biology of the Cell* 19 (11): 4154–66.
584 https://doi.org/10.1091/mbc.E08.

585 Amano, M, K Chihara, K Kimura, Y Fukata, N Nakamura, Y Matsuura, and K Kaibuchi. 1997.
586 "Formation of Actin Stress Fibers and Focal Adhesions Enhanced by Rho-Kinase." *Science*
587 275 (5304): 1308–11. https://doi.org/10.1126/science.275.5304.1308.

588 Amano, Mutsuki, Masaaki Ito, Kazushi Kimura, Yuko Fukata, Kazuyasu Chihara, Takeshi
589 Nakano, Yoshiharu Matsuura, and Kozo Kaibuchi. 1996. "Phosphorylation and Activation
590 of Myosin by Rho-Associated Kinase (Rho-Kinase)." *The Journal of Biological Chemistry*
591 271 (34): 20246–49. https://doi.org/10.1074/jbc.271.34.20246.

592 Arias, Carolina, Ben Weisburd, Noam Stern-Ginossar, Alexandre Mercier, Alexis S Madrid,
593 Priya Bellare, Meghan Holdorf, Jonathan S. Weissman, and Don Ganem. 2014. "KSHV 2.0:
594 A Comprehensive Annotation of the Kaposi's Sarcoma-Associated Herpesvirus Genome
595 Using Next-Generation Sequencing Reveals Novel Genomic and Functional Features."
596 *PLoS Pathogens* 10 (1). https://doi.org/10.1371/journal.ppat.1003847.

597 Asano, Yukako, and Issei Mabuchi. 2001. "Calyculin-A, an Inhibitor for Protein Phosphatases,
598 Induces Cortical Contraction in Unfertilized Sea Urchin Eggs." *Cell Motility and the*
599 *Cytoskeleton* 48 (4): 245–61. https://doi.org/10.1002/cm.1013.

600 Bakheet, Tala, Edward Hitti, and Khalid S A Khabar. 2017. "ARED-Plus: An Updated and
601 Expanded Database of AU-Rich Element-Containing MRNAs and Pre-MRNAs." *Nucleic*
602 *Acids Research* 46 (October 2017): 2017–19. https://doi.org/10.1093/nar/gkx975.

603 Bakheet, Tala, Bryan R G Williams, and Khalid S A Khabar. 2006. "ARED 3.0: The Large and
604 Diverse AU-Rich Transcriptome." *Nucleic Acids Research* 34 (Database issue): D111–14.
605 https://doi.org/10.1093/nar/gkj052.

606 Balinsky, Corey A, Hana Schmeisser, Alexandra I Wells, Sundar Ganesan, Tengchuan Jin,
607 Kavita Singh, and Kathryn C Zoon. 2017. "IRAV (FLJ11286), an Interferon-Stimulated
608 Gene with Antiviral Activity against Dengue Virus, Interacts with MOV10." Edited by
609 Michael S. Diamond. *Journal of Virology* 91 (5). https://doi.org/10.1128/JVI.01606-16.

610 Blanco, Fernando F, Sandhya Sanduja, Natasha G Deane, Perry J Blackshear, and Dan A Dixon.

611 2014. “Transforming Growth Factor β Regulates P-Body Formation through Induction of
612 the MRNA Decay Factor Tristetraprolin.” *Molecular and Cellular Biology* 34 (2): 180–95.
613 https://doi.org/10.1128/MCB.01020-13.
614 Boshoff, Chris, Thomas F Schulz, Margaret M Kennedy, Andrew K Graham, Cyril Fisher, Alero
615 Thomas, J O’D. McGee, Robin a Weiss, and John J O’Leary. 1995. “Kaposi’s Sarcoma-
616 Associated Herpesvirus Infects Endothelial and Spindle Cells.” *Nature Medicine* 1 (12):
617 1274–78. https://doi.org/10.1038/nm1295-1274.
618 Burdick, Ryan, Jessica L Smith, Chawaree Chaipan, Yeshitila Friew, Jianbo Chen, Narasimhan J
619 Venkatachari, Krista A Delviks-Frankenberry, Wei-Shau Hu, and Vinay K. Pathak. 2010.
620 “P Body-Associated Protein Mov10 Inhibits HIV-1 Replication at Multiple Stages.”
621 *Journal of Virology* 84 (19): 10241–53. https://doi.org/10.1128/jvi.00585-10.
622 Burgess, Hannah M., and Ian Mohr. 2015. “Cellular 5′-3′ MRNA Exonuclease Xrn1 Controls
623 Double-Stranded RNA Accumulation and Anti-Viral Responses.” *Cell Host and Microbe*
624 17 (3): 332–44. https://doi.org/10.1016/j.chom.2015.02.003.
625 Burridge, Keith, and Christophe Guilluy. 2016. “Focal Adhesions, Stress Fibers and Mechanical
626 Tension.” *Experimental Cell Research* 343 (1): 14–20.
627 https://doi.org/10.1016/j.yexcr.2015.10.029.
628 Calvo, Fernando, Nil Ege, Araceli Grande-Garcia, Steven Hooper, Robert P. Jenkins, Shahid I.
629 Chaudhry, Kevin Harrington, et al. 2013. “Mechanotransduction and YAP-Dependent
630 Matrix Remodelling Is Required for the Generation and Maintenance of Cancer-Associated
631 Fibroblasts.” *Nature Cell Biology* 15 (6): 637–46. https://doi.org/10.1038/ncb2756.
632 Chang, Y, E Cesarman, M S Pessin, F Lee, J Culpepper, D M Knowles, and P S Moore. 1994.
633 “Identification of Herpes-like DNA Sequences in AIDS-Associated Kaposi’s Sarcoma.”
634 *Science* 266: 1865–69. https://doi.org/10.1126/science.7997879.
635 Chen, C Y, and A B Shyu. 1995. “AU-Rich Elements: Characterization and Importance in
636 MRNA Degradation.” *Trends in Biochemical Sciences* 20 (11): 465–70.
637 https://doi.org/10.1016/S0968-0004(00)89102-1.
638 Ciufo, D M, J S Cannon, L J Poole, F Y Wu, P Murray, R F Ambinder, and G S Hayward. 2001.
639 “Spindle Cell Conversion by Kaposi’s Sarcoma-Associated Herpesvirus: Formation of
640 Colonies and Plaques with Mixed Lytic and Latent Gene Expression in Infected Primary
641 Dermal Microvascular EndCiufo, D. M., Cannon, J. S., Poole, L. J., Wu, F. Y., Murray,

642 P.,." *Journal of Virology* 75 (12): 5614–26. https://doi.org/10.1128/JVI.75.12.5614-
643 5626.2001.
644 Corcoran, Jennifer A, Benjamin P Johnston, and Craig McCormick. 2015. "Viral Activation of
645 MK2-Hsp27-P115RhoGEF-RhoA Signaling Axis Causes Cytoskeletal Rearrangements, P-
646 Body Disruption and ARE-MRNA Stabilization." Edited by Erle S. Robertson. *PLoS*
647 *Pathogens* 11 (1): e1004597. https://doi.org/10.1371/journal.ppat.1004597.
648 Corcoran, Jennifer A, Denys A Khaperskyy, Benjamin P Johnston, Christine A King, David P.
649 Cyr, Alisha V. Olsthoorn, and Craig McCormick. 2012. "Kaposi's Sarcoma-Associated
650 Herpesvirus G-Protein-Coupled Receptor Prevents AU-Rich-Element-Mediated MRNA
651 Decay." *Journal of Virology* 86 (16): 8859–71. https://doi.org/10.1128/JVI.00597-12.
652 Corcoran, Jennifer A, and Craig McCormick. 2015. "Viral Activation of Stress-Regulated Rho-
653 GTPase Signaling Pathway Disrupts Sites of MRNA Degradation to Influence Cellular
654 Gene Expression." *Small GTPases* 6 (4): 178–85.
655 https://doi.org/10.1080/21541248.2015.1093068.
656 Cramer, Louise P, Margaret Siebert, and Timothy J Mitchison. 1997. "Identification of Novel
657 Graded Polarity Actin Filament Bundles in Locomoting Heart Fibroblasts: Implications for
658 the Generation of Motile Force." *Journal of Cell Biology* 136 (6): 1287–1305.
659 https://doi.org/10.1083/jcb.136.6.1287.
660 Cuevas, Rolando A, Arundhati Ghosh, Christina Wallerath, Veit Hornung, Carolyn B Coyne,
661 and Saumendra N Sarkar. 2016. "MOV10 Provides Antiviral Activity against RNA Viruses
662 by Enhancing RIG-I–MAVS-Independent IFN Induction." *The Journal of Immunology* 196
663 (9): 3877–86. https://doi.org/10.4049/jimmunol.1501359.
664 DiMaio, TA, KD Gutierrez, M. Lagunoff. 2011. Latent KSHV infection of endothelial cells
665 induces integrin beta3 to activate angiogenic phenotypes. *PLoS Pathog.* 7:e1002424.
666 Docena, G, L Rovedatti, L Kruidenier, Á Fanning, NAB Leakey, CH Knowles, K Lee, et al.
667 2010. "Down-Regulation of P38 Mitogen-Activated Protein Kinase Activation and
668 Proinflammatory Cytokine Production by Mitogen-Activated Protein Kinase Inhibitors in
669 Inflammatory Bowel Disease." *Clinical and Experimental Immunology* 162 (1): 108–15.
670 https://doi.org/10.1111/j.1365-2249.2010.04203.x.
671 Dupont, Sirio, Leonardo Morsut, Mariaceleste Aragona, Elena Enzo, Stefano Giulitti,
672 Michelangelo Cordenonsi, Francesca Zanconato, et al. 2011. "Role of YAP/TAZ in

673 Mechanotransduction." *Nature* 474 (7350): 179–83. https://doi.org/10.1038/nature10137.
674 Ensoli, B. 1998. "Kaposi's Sarcoma: A Result of the Interplay among Inflammatory Cytokines,
675 Angiogenic Factors and Viral Agents." *Cytokine & Growth Factor Reviews* 9 (1): 63–83.
676 https://doi.org/10.1016/S1359-6101(97)00037-3.
677 Eulalio, Ana, Isabelle Behm-Ansmant, and Elisa Izaurralde. 2007. "P Bodies: At the Crossroads
678 of Post-Transcriptional Pathways." *Nature Reviews Molecular Cell Biology* 8 (1): 9–22.
679 https://doi.org/10.1038/nrm2080.
680 Finch-Edmondson, Megan, and Marius Sudol. 2016. "Framework to Function: Mechanosensitive
681 Regulators of Gene Transcription." *Cellular & Molecular Biology Letters* 21 (1): 28.
682 https://doi.org/10.1186/s11658-016-0028-7.
683 Franks, Tobias M, and Jens Lykke-Andersen. 2007. "TTP and BRF Proteins Nucleate Processing
684 Body Formation to Silence MRNAs with AU-Rich Elements." *Genes and Development* 21
685 (6): 719–35. https://doi.org/10.1101/gad.1494707.
686 Friedland, Julie C, Mark H Lee, and David Boettiger. 2009. "Mechanically Activated Integrin
687 Switch Controls Alpha5 Beta1 Function." *Science* 323 (January): 642–44.
688 "G-Actin / F-Actin In Vivo Assay Kit." n.d. Cytoskeleton Inc.
689 Ganem, Don. 1997. "KSHV and Kaposi's Sarcoma: The End of the Beginning?" *Cell* 91 (2):
690 157–60. https://doi.org/10.1016/S0092-8674(00)80398-0.
691 Garcia, Melissa C, Denise M Ray, Brad Lackford, Mark Rubino, Kenneth Olden, and John D
692 Roberts. 2009. "Arachidonic Acid Stimulates Cell Adhesion through a Novel P38 MAPK-
693 RhoA Signaling Pathway That Involves Heat Shock Protein 27." *Journal of Biological*
694 *Chemistry* 284 (31): 20936–45. https://doi.org/10.1074/jbc.M109.020271.
695 Gill, MB, JE Murphy, JD Fingeroth. 2005. Functional divergence of Kaposi's sarcoma-
696 associated herpesvirus and related gamma-2 herpesvirus thymidine kinases: novel
697 cytoplasmic phosphorylation that alter cellular morphology and disrupt adhesion. *J Virol.*
698 79:14647–59.
699 Gill, MB, R. Turner, PG Stevenson, M. Way. 2015. KSHV-TK is a tyrosine kinase that disrupts
700 focal adhesions and induces Rho-mediated cell contraction. *EMBO J.* 34:448–465.
701 Gomez-Garcia, M Juliana, Amber L Doiron, Robyn RM Steele, Hagar I Labouta, Bahareh
702 Vafadar, Robert D Shepherd, Ian D Gates, David T Cramb, Sarah J Childs, and Kristina D
703 Rinker. 2018. "Nanoparticle Localization in Blood Vessels: Dependence on Fluid Shear

Stress, Flow Disturbances, and Flow-Induced Changes in Endothelial Physiology." *Nanoscale* 10 (32): 15249–61. https://doi.org/10.1039/C8NR03440K.

Grashoff, Carsten, Brenton D Hoffman, Michael D Brenner, Ruobo Zhou, Maddy Parsons, Michael T Yang, Mark A McLean, et al. 2010. "Measuring Mechanical Tension across Vinculin Reveals Regulation of Focal Adhesion Dynamics." *Nature* 466 (7303): 263–66. https://doi.org/10.1038/nature09198.

Grossmann, Claudia, Simona Podgrabinska, Mihaela Skobe, and Don Ganem. 2006. "Activation of NF-KB by the Latent VFLIP Gene of Kaposi's Sarcoma-Associated Herpesvirus Is Required for the Spindle Shape of Virus-Infected Endothelial Cells and Contributes to Their Proinflammatory Phenotype." *Journal of Virology* 80 (14): 7179–85. https://doi.org/10.1128/jvi.01603-05.

Halder, Georg, Sirio Dupont, and Stefano Piccolo. 2012. "Transduction of Mechanical and Cytoskeletal Cues by YAP and TAZ." *Nature Publishing Group* 13 (9): 591–600. https://doi.org/10.1038/nrm3416.

Horvathova I, Voigt F, Kotrys A V., Zhan Y, Artus-Revel CG, Eglinger J, et al. 2017. "The Dynamics of mRNA Turnover Revealed by Single-Molecule Imaging in Single Cells." *Molecular Cell* 68 (3):615-625. https://doi.org/10.1016/j.molcel.2017.09.030

Hotulainen, Pirta, and Pekka Lappalainen. 2006. "Stress Fibers Are Generated by Two Distinct Actin Assembly Mechanisms in Motile Cells." *Journal of Cell Biology* 173 (3): 383–94. https://doi.org/10.1083/jcb.200511093.

Huang, Yu, Li Wang, Jiang Yun Luo, Bochuan Li, Xiao Yu Tian, Li Jing Chen, Yuhong Huang, et al. 2016. "Integrin-YAP/TAZ-JNK Cascade Mediates Atheroprotective Effect of Unidirectional Shear Flow." *Nature* 540 (7634): 579–82. https://doi.org/10.1038/nature20602.

Hubstenberger, Arnaud, Maïté Courel, Marianne Bénard, Sylvie Souquere, Michèle Ernoult-Lange, Racha Chouaib, Zhou Yi, et al. 2017. "P-Body Purification Reveals the Condensation of Repressed MRNA Regulons." *Molecular Cell* 68 (1): 144-157.e5. https://doi.org/10.1016/j.molcel.2017.09.003.

Ishizaki, T, M Uehata, I Tamechika, J Keel, K Nonomura, M Maekawa, and S Narumiya. 2000. "Pharmacological Properties of Y-27632, a Specific Inhibitor of Rho-Associated Kinases." *Molecular Pharmacology* 57 (5): 976–83. http://www.ncbi.nlm.nih.gov/pubmed/10779382.

735 Jackson, Wesley M, Michael J Jaasma, Andrew D Baik, and Tony M Keaveny. 2008. "Over-
736 Expression of Alpha-Actinin with a GFP Fusion Protein Is Sufficient to Increase Whole-
737 Cell Stiffness in Human Osteoblasts." *Annals of Biomedical Engineering* 36 (10): 1605–14.
738 https://doi.org/10.1007/s10439-008-9533-9.
739 Jang, Wonyul, Tackhoon Kim, Ja Seung Koo, Sang-kyum Kim, and Dae-Sik Lim. 2017. "
740 Mechanical Cue-induced YAP Instructs Skp2-dependent Cell Cycle Exit and Oncogenic
741 Signaling ." *The EMBO Journal* 36 (17): 2510–28.
742 https://doi.org/10.15252/embj.201696089.
743 Joshi, Jyotsna, Gautam Mahajan, and Chandrasekhar R. Kothapalli. 2018. "Three-Dimensional
744 Collagenous Niche and Azacytidine Selectively Promote Time-Dependent
745 Cardiomyogenesis from Human Bone Marrow-Derived MSC Spheroids." *Biotechnology*
746 *and Bioengineering* 115 (8): 2013–26. https://doi.org/10.1002/bit.26714.
747 Julian, Linda, and Michael F Olson. 2014. "Rho-Associated Coiled-Coil Containing Kinases
748 (ROCK)." *Small GTPases* 5 (2): e29846. https://doi.org/10.4161/sgtp.29846.
749 Kamentsky, Lee, Thouis R Jones, Adam Fraser, Mark-Anthony Bray, David J Logan, Katherine
750 L Madden, Vebjorn Ljosa, Curtis Rueden, Kevin W Eliceiri, and Anne E Carpenter. 2011.
751 "Improved Structure, Function and Compatibility for CellProfiler: Modular High-
752 Throughput Image Analysis Software." *Bioinformatics (Oxford, England)* 27 (8): 1179–80.
753 https://doi.org/10.1093/bioinformatics/btr095.
754 Kapoor, Avnish, Wantong Yao, Haoqiang Ying, Sujun Hua, Alison Liewen, Qiuyun Wang, Yi
755 Zhong, et al. 2014. "Yap1 Activation Enables Bypass of Oncogenic KRAS Addiction in
756 Pancreatic Cancer." *Cell* 158 (1): 185–97. https://doi.org/10.1016/j.cell.2014.06.003.
757 Katoh, K, Y Kano, M Masuda, H Onishi, and K Fujiwara. 1998. "Isolation and Contraction of
758 the Stress Fiber." *Molecular Biology of the Cell* 9 (7): 1919–38.
759 https://doi.org/10.1091/mbc.9.7.1919.
760 Kedersha, Nancy, and Paul Anderson. 2007. "Mammalian Stress Granules and Processing
761 Bodies." *Methods in Enzymology* 431 (07): 61–81. https://doi.org/10.1016/S0076-
762 6879(07)31005-7.
763 Kedersha, Nancy, Sarah Tisdale, Tyler Hickman, and Paul Anderson. 2008. *Chapter 26 Real-*
764 *Time and Quantitative Imaging of Mammalian Stress Granules and Processing Bodies*.
765 *Methods in Enzymology*. 1st ed. Vol. 448. Elsevier Inc. https://doi.org/10.1016/S0076-

766 6879(08)02626-8.
767 Kimura, K, M Ito, M Amano, K Chihara, Y Fukata, M Nakafuku, B Yamamori, et al. 1996.
768 "Regulation of Myosin Phosphatase by Rho and Rho-Associated Kinase (Rho-Kinase)."
769 *Science (New York, N.Y.)* 273 (5272): 245–48.
770 https://doi.org/10.1126/science.273.5272.245.
771 Kimura, Masahiro, Takahiro Horie, Osamu Baba, Yuya Ide, Shuhei Tsuji, Randolph Ruiz
772 Rodriguez, Toshimitsu Watanabe, et al. 2020. "Homeobox A4 Suppresses Vascular
773 Remodeling by Repressing YAP/TEAD Transcriptional Activity." *EMBO Reports* 21 (4):
774 e48389. https://doi.org/10.15252/embr.201948389.
775 Kong, Fang, Andrés J García, A Paul Mould, Martin J Humphries, and Cheng Zhu. 2009.
776 "Demonstration of Catch Bonds between an Integrin and Its Ligand." *Journal of Cell*
777 *Biology* 185 (7): 1275–84. https://doi.org/10.1083/jcb.200810002.
778 Kovacs, M, J Toth, C Hetenyi, A Malnasi-Csizmadia, and JR Sellers. 2004. "Mechanism of
779 Blebbistatin Inhibition of Myosin II." *Journal of Biological Chemistry* 279 (34): 35557–63.
780 https://doi.org/10.1074/jbc.M405319200.
781 Lagunoff, M. 2015. KSHV-TK: Thymidine kinase or tyrosine kinase? EMBO J. 34 (4): 427–9.
782 Lai, Jason Kuan Han, and Didier Y.R. Stainier. 2017. "Pushing Yap into the Nucleus with Shear
783 Force." *Developmental Cell* 40 (6): 517–18. https://doi.org/10.1016/j.devcel.2017.03.008.
784 Lazarides, Elias, and Keith Burridge. 1975. "α-Actinin: Immunofluorescent Localization of a
785 Muscle Structural Protein in Nonmuscle Cells." *Cell* 6 (3): 289–98.
786 https://doi.org/10.1016/0092-8674(75)90180-4.
787 Lee, Byoungkoo, Xin Zhou, Kristin Riching, Kevin W Eliceiri, Patricia J Keely, Scott A
788 Guelcher, Alissa M Weaver, and Yi Jiang. 2014. "A Three-Dimensional Computational
789 Model of Collagen Network Mechanics." Edited by Sanjay Kumar. *PLoS ONE* 9 (11):
790 e111896. https://doi.org/10.1371/journal.pone.0111896.
791 Lee, Hyun Jung, Miguel F Diaz, Katherine M Price, Joyce A Ozuna, Songlin Zhang, Eva M
792 Sevick-Muraca, John P. Hagan, and Pamela L. Wenzel. 2017. "Fluid Shear Stress Activates
793 YAP1 to Promote Cancer Cell Motility." *Nature Communications* 8 (1): 14122.
794 https://doi.org/10.1038/ncomms14122.
795 Lee, JSH. 2006. "Ballistic Intracellular Nanorheology Reveals ROCK-Hard Cytoplasmic
796 Stiffening Response to Fluid Flow." *Journal of Cell Science* 119 (9): 1760–68.

https://doi.org/10.1242/jcs.02899.

Lee, Stacey, and Sanjay Kumar. 2016. "Actomyosin Stress Fiber Mechanosensing in 2D and 3D." *F1000Research* 5 (0): 2261. https://doi.org/10.12688/f1000research.8800.1.

Li, Ying, Rui Chen, Qian Zhou, Zhisheng Xu, Chao Li, Shuai Wang, Aiping Mao, Xiaodong Zhang, Weiwu He, and Hong Bing Shu. 2012. "LSm14A Is a Processing Body-Associated Sensor of Viral Nucleic Acids That Initiates Cellular Antiviral Response in the Early Phase of Viral Infection." *Proceedings of the National Academy of Sciences of the United States of America* 109 (29): 11770–75. https://doi.org/10.1073/pnas.1203405109.

Liu, G, FX Yu, YC Kim, Z. Meng, J Naipauer, DJ Looney, X Liu, JS Gutkind, EA Mesri, and K L Guan. 2015. "Kaposi Sarcoma-Associated Herpesvirus Promotes Tumorigenesis by Modulating the Hippo Pathway." *Oncogene* 34 (27): 3536–46. https://doi.org/10.1038/onc.2014.281.

Liu, Huan, Xiaoming Dai, Xiaolei Cao, Huan Yan, Xinyan Ji, Haitao Zhang, Shuying Shen, et al. 2018. "PRDM4 Mediates YAP-induced Cell Invasion by Activating Leukocyte-specific Integrin B2 Expression." *EMBO Reports* 19 (6): 1–14. https://doi.org/10.15252/embr.201745180.

Lumb, Jennifer H, Lauren M Popov, Siyuan Ding, Marie T Keith, Bryan D Merrill, Harry B Greenberg, Jan E. Carette, Qin Li, and Jin Billy Li. 2017. "DDX6 Represses Aberrant Activation of Interferon-Stimulated Genes." *Cell Reports* 20 (4): 819–31. https://doi.org/10.1016/j.celrep.2017.06.085.

McCormick, Craig, and Don Ganem. 2005. "The Kaposin B Protein of KSHV Activates the P38/MK2 Pathway and Stabilizes Cytokine MRNAs." *Science* 307 (5710): 739–41. https://doi.org/10.1126/science.1105779.

Mo, Jung Soon, Zhipeng Meng, Young Chul Kim, Hyun Woo Park, Carsten Gram Hansen, Soohyun Kim, Dae Sik Lim, and Kun Liang Guan. 2015. "Cellular Energy Stress Induces AMPK-Mediated Regulation of YAP and the Hippo Pathway." *Nature Cell Biology* 17 (4): 500–510. https://doi.org/10.1038/ncb3111.

Montaner, Silvia, Akrit Sodhi, Amanda K. Ramsdell, Daniel Martin, Jiadi Hu, Earl T Sawai, and J. Silvio Gutkind. 2006. "The Kaposi's Sarcoma-Associated Herpesvirus G Protein-Coupled Receptor as a Therapeutic Target for the Treatment of Kaposi's Sarcoma." *Cancer Research* 66 (1): 168–74. https://doi.org/10.1158/0008-5472.CAN-05-1026.

828 Moreno-Vicente, Roberto, Dácil María Pavón, Inés Martín-Padura, Mauro Català-Montoro,
829 Alberto Díez-Sánchez, Antonio Quílez-Álvarez, Juan Antonio López, et al. 2018.
830 "Caveolin-1 Modulates Mechanotransduction Responses to Substrate Stiffness through
831 Actin-Dependent Control of YAP." *Cell Reports* 25 (6): 1622-1635.e6.
832 https://doi.org/10.1016/j.celrep.2018.10.024.
833 Nakajima, Hiroyuki, and Naoki Mochizuki. 2017. "Flow Pattern-Dependent Endothelial Cell
834 Responses through Transcriptional Regulation." *Cell Cycle* 16 (20): 1893–1901.
835 https://doi.org/10.1080/15384101.2017.1364324.
836 Nakajima, Hiroyuki, Kimiko Yamamoto, Sobhika Agarwala, Kenta Terai, Hajime Fukui,
837 Shigetomo Fukuhara, Koji Ando, et al. 2017. "Flow-Dependent Endothelial YAP
838 Regulation Contributes to Vessel Maintenance." *Developmental Cell* 40 (6): 523-536.e6.
839 https://doi.org/10.1016/j.devcel.2017.02.019.
840 Naranatt, Pramod P, Shaw M. Akula, Christopher A Zien, Harinivas H Krishnan, and Bala
841 Chandran. 2003. "Kaposi's Sarcoma-Associated Herpesvirus Induces the
842 Phosphatidylinositol 3-Kinase-PKC-ζ-MEK-ERK Signaling Pathway in Target Cells Early
843 during Infection: Implications for Infectivity." *Journal of Virology* 77 (2): 1524–39.
844 https://doi.org/10.1128/jvi.77.2.1524-1539.2003.
845 Ng, Chen Seng, Dacquin M Kasumba, Takashi Fujita, and Honglin Luo. 2020. "Spatio-Temporal
846 Characterization of the Antiviral Activity of the XRN1-DCP1/2 Aggregation against
847 Cytoplasmic RNA Viruses to Prevent Cell Death." *Cell Death and Differentiation*.
848 https://doi.org/10.1038/s41418-020-0509-0.
849 Noria, Sabrena, Feng Xu, Shannon McCue, Mara Jones, Avrum I Gotlieb, and B Lowell
850 Langille. 2004. "Assembly and Reorientation of Stress Fibers Drives Morphological
851 Changes to Endothelial Cells Exposed to Shear Stress." *The American Journal of Pathology*
852 164 (4): 1211–23. https://doi.org/10.1016/S0002-9440(10)63209-9.
853 Núñez, Rocío Daviña, Matthias Budt, Sandra Saenger, Katharina Paki, Ulrike Arnold, Anne
854 Sadewasser, and Thorsten Wolff. 2018. "The RNA Helicase DDX6 Associates with RIG-I
855 to Augment Induction of Antiviral Signaling." *International Journal of Molecular Sciences*
856 19 (7): 1–14. https://doi.org/10.3390/ijms19071877.
857 Ohashi, Kazumasa, Kyoko Nagata, Midori Maekawa, Toshimasa Ishizaki, Shuh Narumiya, and
858 Kensaku Mizuno. 2000. "Rho-Associated Kinase ROCK Activates LIM-Kinase 1 by

859 Phosphorylation at Threonine 508 within the Activation Loop." *Journal of Biological*
860 *Chemistry* 275 (5): 3577–82. https://doi.org/10.1074/jbc.275.5.3577.
861 Ojala, Päivi M, and Thomas F Schulz. 2014. "Manipulation of Endothelial Cells by KSHV:
862 Implications for Angiogenesis and Aberrant Vascular Differentiation." *Seminars in Cancer*
863 *Biology* 26 (June): 69–77. https://doi.org/10.1016/j.semcancer.2014.01.008.
864 Ostareck, Dirk H, Isabel S Naarmann-de Vries, and Antje Ostareck-Lederer. 2014. "DDX6 and
865 Its Orthologs as Modulators of Cellular and Viral RNA Expression." *Wiley Interdisciplinary*
866 *Reviews: RNA* 5 (5): 659–78. https://doi.org/10.1002/wrna.1237.
867 Panciera, Tito, Luca Azzolin, Atsushi Fujimura, Daniele Di Biagio, Chiara Frasson, Silvia
868 Bresolin, Sandra Soligo, et al. 2016. "Induction of Expandable Tissue-Specific
869 Stem/Progenitor Cells through Transient Expression of YAP/TAZ." *Cell Stem Cell* 19 (6):
870 725–37. https://doi.org/10.1016/j.stem.2016.08.009.
871 Pavel, Mariana, Maurizio Renna, So Jung Park, Fiona M Menzies, Thomas Ricketts, Jens
872 Füllgrabe, Avraham Ashkenazi, et al. 2018. "Contact Inhibition Controls Cell Survival and
873 Proliferation via YAP/TAZ-Autophagy Axis." *Nature Communications* 9 (1).
874 https://doi.org/10.1038/s41467-018-05388-x.
875 Pellegrin, S, and H Mellor. 2007. "Actin Stress Fibres." *Journal of Cell Science* 120 (20): 3491–
876 99. https://doi.org/10.1242/jcs.018473.
877 Pollard, Thomas D. 2016. "Actin and Actin-Binding Proteins." *Cold Spring Harbor Perspectives*
878 *in Biology* 8 (8): a018226. https://doi.org/10.1101/cshperspect.a018226.
879 Ridley, Anne J, and Alan Hall. 1992. "The Small GTP-Binding Protein Rho Regulates the
880 Assembly of Focal Adhesions and Actin Stress Fibers in Response to Growth Factors." *Cell*
881 70 (3): 389–99. https://doi.org/10.1016/0092-8674(92)90163-7.
882 Rio, Armando del, Raul Perez-Jimenez, Ruchuan Liu, Pere Roca-Cusachs, Julio M Fernandez,
883 and Michael P Sheetz. 2009. "Stretching Single Talin Rod." *Science* 323 (5914): 638–41.
884 Russo, James J, Roy A Bohenzky, MC Chien, Jing Chen, Ming Yan, Dawn Maddalena, J Preston
885 Parry, et al. 1996. "Nucleotide Sequence of the Kaposi Sarcoma-Associated Herpesvirus
886 (HHV8)." *Proceedings of the National Academy of Sciences* 93 (25): 14862–67.
887 https://doi.org/10.1073/pnas.93.25.14862.
888 Schmitz, Arndt AP, Eve-Ellen Govek, Benjamin Böttner, and Linda Van Aelst. 2000. "Rho
889 GTPases: Signaling, Migration, and Invasion." *Experimental Cell Research* 261 (1): 1–12.

https://doi.org/10.1006/excr.2000.5049.

Sharma, Nishi R, Vladimir Majerciak, Michael J Kruhlak, Lulu Yu, Jeong Gu Kang, Acong Yang, Shuo Gu, Marvin J Fritzler, and Zhi-ming Zheng. 2019. "KSHV RNA-Binding Protein ORF57 Inhibits P-Body Formation to Promote Viral Multiplication by Interaction with Ago2 and GW182," 1–18. https://doi.org/10.1093/nar/gkz683.

Shaw, Gray, and Robert Kamen. 1986. "A Conserved AU Sequence from the 3′ Untranslated Region of GM-CSF MRNA Mediates Selective MRNA Degradation." *Cell* 46 (5): 659–67. https://doi.org/10.1016/0092-8674(86)90341-7.

Shen, Zhewei, and Ben Z Stanger. 2015. "YAP Regulates S-Phase Entry in Endothelial Cells." Edited by Deanna M Koepp. *PLOS ONE* 10 (1): e0117522. https://doi.org/10.1371/journal.pone.0117522.

Shepard, LW, M. Yang, P Xie, DD Browning, T Voyno-Yasenetskaya, T Kozasa, RD Ye. 2001. Constitutive activation of NF-kappa B and secretion of interleukin-8 induced by the G protein-coupled receptor of Kaposi's sarcoma-associated herpesvirus involve G alpha(13) and RhoA. *J Biol Chem*. 276 (49):45979-87.

Sheth, Ujwal. 2003. "Decapping and Decay of Messenger RNA Occur in Cytoplasmic Processing Bodies." *Science* 300 (5620): 805–8. https://doi.org/10.1126/science.1082320.

Shyu, AB, ME Greenberg, and JG Belasco. 1989. "The C-Fos Transcript Is Targeted for Rapid Decay by Two Distinct MRNA Degradation Pathways." *Genes & Development* 3 (1): 60–72. https://doi.org/10.1101/gad.3.1.60.

Small, J Victor, K Rottner, I Kaverina, and KI Anderson. 1998. "Assembling an Actin Cytoskeleton for Cell Attachment and Movement." *Biochimica et Biophysica Acta - Molecular Cell Research* 1404 (3): 271–81. https://doi.org/10.1016/S0167-4889(98)00080-9.

Speck, Samuel H, and Don Ganem. 2010. "Viral Latency and Its Regulation: Lessons from the γ-Herpesviruses." *Cell Host and Microbe* 8 (1): 100–115. https://doi.org/10.1016/j.chom.2010.06.014.

Staskus, K A, W Zhong, K Gebhard, B Herndier, H Wang, R Renne, J Beneke, et al. 1997. "Kaposi's Sarcoma-Associated Herpesvirus Gene Expression in Endothelial (Spindle) Tumor Cells." *Journal of Virology* 71 (1): 715–19. https://doi.org/10.1128/jvi.71.1.715-719.1997.

921 Stoecklin, Georg, Thomas Mayo, and Paul Anderson. 2006. "ARE-MRNA Degradation Requires
922 the 5'-3' Decay Pathway." *EMBO Reports* 7 (1): 72–77.
923 https://doi.org/10.1038/sj.embor.7400572.
924 Sugimoto, Wataru, Katsuhiko Itoh, Yasumasa Mitsui, Takahiro Ebata, Hideaki Fujita, Hiroaki
925 Hirata, and Keiko Kawauchi. 2018. "Substrate Rigidity-Dependent Positive Feedback
926 Regulation between YAP and ROCK2." *Cell Adhesion and Migration* 12 (2): 101–8.
927 https://doi.org/10.1080/19336918.2017.1338233.
928 Takahashi, Shinya, Kyoko Sakurai, Arisa Ebihara, Hiroaki Kajiho, Kota Saito, Kenji Kontani,
929 Hiroshi Nishina, and Toshiaki Katada. 2011. "RhoA Activation Participates in
930 Rearrangement of Processing Bodies and Release of Nucleated AU-Rich MRNAs." *Nucleic*
931 *Acids Research* 39 (8): 3446–57. https://doi.org/10.1093/nar/gkq1302.
932 Tan, John L, Joe Tien, Dana M Pirone, Darren S Gray, Kiran Bhadriraju, and Christopher S
933 Chen. 2003. "Cells Lying on a Bed of Microneedles: An Approach to Isolate Mechanical
934 Force." *Proceedings of the National Academy of Sciences* 100 (4): 1484–89.
935 https://doi.org/10.1073/pnas.0235407100.
936 Tojkander, Sari, Gergana Gateva, and Pekka Lappalainen. 2012. "Actin Stress Fibers -
937 Assembly, Dynamics and Biological Roles." *Journal of Cell Science* 125 (Pt 8): 1855–64.
938 https://doi.org/10.1242/jcs.098087.
939 Tutucci, Evelina, Maria Vera, Jeetayu Biswas, Jennifer Garcia, Roy Parker, and Robert H.
940 Singer. 2018. "An Improved MS2 System for Accurate Reporting of the MRNA Life
941 Cycle." *Nature Methods* 15 (1): 81–89. https://doi.org/10.1038/nmeth.4502.
942 Umbach, Jennifer L, Hui Ling Yen, Leo L M Poon, and Bryan R Cullen. 2010. "Influenza a
943 Virus Expresses High Levels of an Unusual Class of Small Viral Leader RNAs in Infected
944 Cells." *MBio* 1 (4): 1–8. https://doi.org/10.1128/mBio.00204-10.
945 Vallenius, Tea. 2013. "Actin Stress Fibre Subtypes in Mesenchymal-Migrating Cells." *Open*
946 *Biology* 3 (6): 130001. https://doi.org/10.1098/rsob.130001.
947 Vassilev, Alex, Kotaro J Kaneko, Hongjun Shu, Yingming Zhao, and Melvin L. DePamphilis.
948 2001. "TEAD/TEF Transcription Factors Utilize the Activation Domain of YAP65, a
949 Src/Yes-Associated Protein Localized in the Cytoplasm." *Genes and Development* 15 (10):
950 1229–41. https://doi.org/10.1101/gad.888601.
951 Vindry, Caroline, Aline Marnef, Helen Broomhead, Laure Twyffels, Sevim Ozgur, Georg

Stoecklin, Miriam Llorian, et al. 2017. “Dual RNA Processing Roles of Pat1b via Cytoplasmic Lsm1-7 and Nuclear Lsm2-8 Complexes.” *Cell Reports* 20 (5): 1187–1200. https://doi.org/10.1016/j.celrep.2017.06.091.

Vozzi, Federico, Jonica Campolo, Lorena Cozzi, Gianfranco Politano, Stefano Di Carlo, Michela Rial, Claudio Domenici, and Oberdan Parodi. 2018. “Computing of Low Shear Stress-Driven Endothelial Gene Network Involved in Early Stages of Atherosclerotic Process.” *BioMed Research International* 2018 (September): 1–12. https://doi.org/10.1155/2018/5359830.

Wada, KI, K Itoga, T Okano, S Yonemura, and H Sasaki. 2011. “Hippo Pathway Regulation by Cell Morphology and Stress Fibers.” *Development* 138 (18): 3907–14. https://doi.org/10.1242/dev.070987.

Wang, Huanru, Liang Chang, Xiaohui Wang, Airong Su, Chunhong Feng, Yuxuan Fu, Deyan Chen, Nan Zheng, and Zhiwei Wu. 2016. “MOV10 Interacts with Enterovirus 71 Genomic 5′UTR and Modulates Viral Replication.” *Biochemical and Biophysical Research Communications* 479 (3): 571–77. https://doi.org/10.1016/j.bbrc.2016.09.112.

Wang, Kuei-Chun, Yi-Ting Yeh, Phu Nguyen, Elaine Limqueco, Jocelyn Lopez, Satenick Thorossian, Kun-Liang Guan, Yi-Shuan J. Li, and Shu Chien. 2016. “Flow-Dependent YAP/TAZ Activities Regulate Endothelial Phenotypes and Atherosclerosis.” *Proceedings of the National Academy of Sciences* 113 (41): 11525–30. https://doi.org/10.1073/pnas.1613121113.

Watanabe, Naoki, Takayuki Kato, Akiko Fujita, Toshimasa Ishizaki, and Shuh Narumiya. 1999. “Cooperation between MDia1 and ROCK in Rho-Induced Actin Reorganization.” *Nature Cell Biology* 1 (3): 136–43. https://doi.org/10.1038/11056.

Watanabe, Naoki, Pascal Madaule, Tim Reid, Toshimasa Ishizaki, Go Watanabe, Akira Kakizuka, Yuji Saito, Kazuwa Nakao, Brigitte M. Jockusch, and Shuh Narumiya. 1997. “P140mDia, a Mammalian Homolog of Drosophila Diaphanous, Is a Target Protein for Rho Small GTPase and Is a Ligand for Profilin.” *EMBO Journal* 16 (11): 3044–56. https://doi.org/10.1093/emboj/16.11.3044.

Wilbertz, Johannes H, Franka Voigt, Ivana Horvathova, Gregory Roth, Yinxiu Zhan, and Jeffrey A. Chao. 2019. “Single-Molecule Imaging of MRNA Localization and Regulation during the Integrated Stress Response.” *Molecular Cell* 73 (5): 946-958.e7.

983 https://doi.org/10.1016/j.molcel.2018.12.006.
984 Winzen, Reinhard, Michael Kracht, Birgit Ritter, Arno Wilhelm, Chyi Ying A Chen, Ann Bin
985 Shyu, Monika Müller, Matthias Gaestel, Klaus Resch, and Helmut Holtmann. 1999. "The
986 P38 MAP Kinase Pathway Signals for Cytokine-Induced MRNA Stabilization via MAP
987 Kinase-Activated Protein Kinase 2 and an AU-Rich Region-Targeted Mechanism." *EMBO*
988 *Journal* 18 (18): 4969–80. https://doi.org/10.1093/emboj/18.18.4969.
989 Yang, Chih-Sheng, Eleni Stampouloglou, Nathan M Kingston, Liye Zhang, Stefano Monti, and
990 Xaralabos Varelas. 2018. "Glutamine-utilizing Transaminases Are a Metabolic
991 Vulnerability of TAZ/YAP-activated Cancer Cells." *EMBO Reports* 19 (6): 1–11.
992 https://doi.org/10.15252/embr.201643577.
993 Yang, Ya Li, Lindsay M. Leone, and Laura J. Kaufman. 2009. "Elastic Moduli of Collagen Gels
994 Can Be Predicted from Two-Dimensional Confocal Microscopy." *Biophysical Journal* 97
995 (7): 2051–60. https://doi.org/10.1016/j.bpj.2009.07.035.
996 Yu, Fa Xing, Bin Zhao, Nattapon Panupinthu, Jenna L. Jewell, Ian Lian, Lloyd H. Wang,
997 Jiagang Zhao, et al. 2012. "Regulation of the Hippo-YAP Pathway by G-Protein-Coupled
998 Receptor Signaling." *Cell* 150 (4): 780–91. https://doi.org/10.1016/j.cell.2012.06.037.
999 Yu, Jiang Hong, Wei-Hong Yang, Tod Gulick, Kenneth D Bloch, and Donald B Bloch. 2005.
1000 "Ge-1 Is a Central Component of the Mammalian Cytoplasmic MRNA Processing Body."
1001 *RNA (New York, N.Y.)* 11 (12): 1795–1802. https://doi.org/10.1261/rna.2142405.
1002 Zanconato, Francesca, Mattia Forcato, Giusy Battilana, Luca Azzolin, Erika Quaranta, Beatrice
1003 Bodega, Antonio Rosato, Silvio Bicciato, Michelangelo Cordenonsi, and Stefano Piccolo.
1004 2015. "Genome-Wide Association between YAP/TAZ/TEAD and AP-1 at Enhancers
1005 Drives Oncogenic Growth." *Nature Cell Biology* 17 (9): 1218–27.
1006 https://doi.org/10.1038/ncb3216.
1007 Zhang, Qian, Fansen Meng, Shasha Chen, Steven W Plouffe, Shiying Wu, Shengduo Liu, Xinran
1008 Li, et al. 2017. "Hippo Signalling Governs Cytosolic Nucleic Acid Sensing through YAP /
1009 TAZ-Mediated TBK1 Blockade." *Nature Cell Biology* 19 (4): 362–74.
1010 https://doi.org/10.1038/ncb3496.
1011 Zhao, Bin, Li Li, Lloyd Wang, Cun Yu Wang, Jindan Yu, and Kun Liang Guan. 2012. "Cell
1012 Detachment Activates the Hippo Pathway via Cytoskeleton Reorganization to Induce
1013 Anoikis." *Genes and Development* 26 (1): 54–68. https://doi.org/10.1101/gad.173435.111.

1014 Zhao, Bin, Bin Zhao, Xiaomu Wei, Xiaomu Wei, Weiquan Li, Weiquan Li, Ryan S Udan, et al.
1015 2007. "Inactivation of YAP Oncoprotein by the Hippo Pathway Is Involved in Cell Contact
1016 Inhibition and Tissue Growth Control." *Genes and Development* 21: 2747–61.
1017 https://doi.org/10.1101/gad.1602907.Hpo/Sav.
1018 Zhong, W, H Wang, B Herndier, and D Ganem. 1996. "Restricted Expression of Kaposi
1019 Sarcoma-Associated Herpesvirus (Human Herpesvirus 8) Genes in Kaposi Sarcoma."
1020 *Proceedings of the National Academy of Sciences of the United States of America* 93 (13):
1021 6641–46. https://doi.org/10.1073/pnas.93.13.6641.
1022
1023
1024

Acknowledgements

We would like to sincerely thank the members of the Corcoran lab for helpful discussions about this work. We would like to thank Dr. Craig McCormick (Dalhousie University) for helpful discussions on this manuscript and his lab for plasmids, expertise and invaluable advice. We would like to thank Mr. Stephen Whitefield of the Dalhousie *CORES* Cellular and Molecular Digital Imaging Facility and Dr. Anne Vaahtokari of the Charbonneau Microscopy Facility, UCalgary for microscopy support. ELC was supported by a Killam predoctoral scholarship, an NSERC CGS-M scholarship, and a Nova Scotia Graduate scholarship. Operating funds to support this work derive from an NSERC Discovery grant RGPIN-2015-04882 to JAC.

Competing Interests

The authors have no competing interests to declare.

1040 **Figure Legends**
1041

1042 **Figure 1: The RhoA-effector mDia1 is required for KapB-mediated PB disassembly.** KapB-
1043 and vector- expressing HUVECs were transduced with shRNAs targeting mDia1 (shDIA1-1,
1044 shDIA1-2) or with a non-targeting (shNT) control and selected. In parallel, cells were fixed for
1045 immunofluorescence or lysed for immunoblotting. (A) One representative immunoblot of three
1046 independent experiments stained with mDia1-specific antibody is shown. (B, C) Fixed cells were
1047 stained for CellProfiler analysis as detailed in the methods. (B) The number of EDC4 puncta per
1048 cell was quantified and normalized to the vector NT control within each replicate. (C)
1049 CellProfiler data was used to calculate the ratio of EDC4 puncta counts in KapB-expressing cells
1050 versus the vector control for each treatment condition. (D) Representative images of cells stained
1051 for PB-resident protein EDC4 (green), KapB (blue), and F-actin (red, phalloidin). Boxes indicate
1052 area shown in the EDC4 (zoom) panel. Scale bar represents 20 μm. Statistics were determined
1053 using ratio paired t-tests between control and experimental groups; error bars represent standard
1054 deviation; n=3 independent biological replicates; * = $p < 0.05$, ** = $p < 0.01$.
1055

1056 **Figure 2: The RhoA-effector ROCK is required for KapB-mediated PB disassembly.** (A-C)
1057 KapB- and vector- expressing HUVECs were treated with 10 μM Y-27632 or water control for 4
1058 h and fixed for immunofluorescence. (A) Representative images of cells stained for PB-resident
1059 protein EDC4 (green), KapB (blue), and F-actin (red, phalloidin). Boxes indicate area shown in
1060 the EDC4 (zoom) panel. Scale bar represents 20 μm. (B, C) Fixed cells were stained for
1061 CellProfiler analysis as detailed in the methods. (B) The number of EDC4 puncta per cell was
1062 quantified and normalized to the vector NT control within each replicate. (C) CellProfiler data
1063 was used to calculate the ratio of EDC4 puncta counts in KapB-expressing cells versus the vector
1064 control for each treatment condition. (D-F) KapB- and vector- expressing HUVECs were
1065 transduced with shRNAs targeting ROCK1 and ROCK2 (shROCK1-1, shROCK1-2, shROCK2-
1066 1, shROCK2-2) or with a non-targeting (shNT) control and selected. Cells were fixed for
1067 immunofluorescence. (D, E) Fixed cells were stained for CellProfiler analysis as detailed in the
1068 methods. (D) The number of EDC4 puncta per cell was quantified and normalized to the vector
1069 NT control within each replicate. (E) CellProfiler data was used to calculate the ratio of EDC4
1070 puncta counts in KapB-expressing cells versus the vector control for each treatment condition.

1071 (F) Representative images of cells stained for PB-resident protein EDC4 (green), KapB (blue),
1072 and F-actin (red, phalloidin). Boxes indicate images shown in EDC4 (zoom) panel. Scale bar
1073 represents 20 μm. Statistics were determined using ratio paired t-tests between control and
1074 experimental groups; error bars represent standard deviation from n=3 independent biological
1075 replicates except shROCK1-2, (n=2); * = $p < 0.05$, ** = $p < 0.01$.
1076
1077 **Figure 3: Actomyosin contractility controls PB disassembly.** (A-C) KapB- and vector-
1078 expressing HUVECs were treated with 10μM blebbistatin to inhibit actomyosin contractility or
1079 DMSO for 30 min and fixed for immunofluorescence. (A, B) Fixed cells were stained for
1080 CellProfiler analysis as detailed in the methods. (A) The number of EDC4 puncta per cell was
1081 quantified and normalized to the vector NT control within each replicate. (B) CellProfiler data
1082 was used to calculate the ratio of EDC4 puncta counts in KapB-expressing cells versus the vector
1083 control for each treatment condition. (C) Representative images of cells stained for PB-resident
1084 protein EDC4 (green), KapB (blue), and F-actin (red, phalloidin). Boxes indicate area shown in
1085 the EDC4 (zoom) panel. Scale bar represents 20 μm. (D, E) Untransduced HUVECs were treated
1086 with 5 nM Calyculin A (CalA) to stimulate actomyosin contraction or DMSO for 20 min and
1087 fixed for immunofluorescence. (D) Fixed cells were stained for CellProfiler analysis as detailed
1088 in the methods. EDC4 puncta per cell were quantified and normalized to the DMSO control
1089 within each replicate. (E) Representative images of cells treated with 5 nM CalA and stained for
1090 PB-resident protein EDC4 (green) and F-actin (red, phalloidin). Boxes indicate area shown in the
1091 EDC4 (zoom) panel. Scale bar represents 20 μm. Statistics were determined using ratio paired t-
1092 tests between control and experimental groups; error bars represent standard deviation; n=3 (A,
1093 B) and n=5 (D) independent biological replicates; * = $p < 0.05$.
1094
1095 **Figure 4: YAP is required for KapB-mediated PB disassembly.** KapB- and vector-
1096 expressing HUVECs were transduced with shRNAs targeting YAP (shYAP-1, shYAP-2) or with
1097 a non-targeting (shNT) control and selected. In parallel, cells were fixed for immunofluorescence
1098 or lysed for immunoblotting. (A) One representative immunoblot of three independent
1099 experiments stained with YAP-specific antibody is shown. (B-D) Fixed cells were stained for
1100 CellProfiler analysis as detailed in the methods. (B) The number of EDC4 puncta per cell was
1101 quantified and normalized to the vector NT control within each replicate. (C) CellProfiler data

1102 was used to calculate the ratio of EDC4 puncta count in KapB-expressing cells to the vector
1103 control for each treatment condition. (D) Representative images of cells stained for PB-resident
1104 protein EDC4 (green), KapB (blue), and F-actin (red, phalloidin). Boxes indicate area shown in
1105 the EDC4 (zoom) panel. Scale bar represents 20 μm. Statistics were determined using ratio
1106 paired t-tests between control and experimental groups; error bars represent standard deviation;
1107 n=3 independent biological replicates; * = $p < 0.05$, ** = $p < 0.01$, *** = $p < 0.001$.
1108
1109 **Figure 5: Active YAP elicits PB disassembly.** HUVECs were transduced with YAP 5SA-
1110 expressing and empty vector lentivirus and selected. Cells were fixed for immunofluorescence.
1111 (A) Representative images of cells stained for PB-resident protein EDC4 (green) and F-actin
1112 (red, phalloidin). Boxes indicate area shown in the EDC4 (zoom) panel. Scale bar represents 20
1113 μm. (B) Fixed cells were stained for CellProfiler analysis as detailed in the methods. The number
1114 of EDC4 puncta per cell was quantified and normalized to the vector control. (C-E)
1115 Representative images of cells stained for (C) DDX6 (red), DCP1a (green) and DAPI (blue), (D)
1116 DDX6 (red), EDC4 (green) and DAPI (blue), and (E) DDX6 (red), YAP (green) and DAPI
1117 (blue). Boxes indicate area shown in the zoom panels. Scale bar represents 20 μm. Statistics
1118 were determined using ratio paired t-tests between control and experimental groups (B); error
1119 bars represent standard deviation; n=3 independent biological replicates; * = $p < 0.05$, ** = $p <$
1120 0.01.
1121
1122 **Figure 6: YAP transcriptional activity is required for PB disassembly.** HUVECs were
1123 transduced with YAP 5SA-, YAP 6SA- or vector-expressing lentivirus and selected. Cells were
1124 fixed for immunofluorescence. (A) Representative images of cells stained for EDC4 (red),
1125 DDX6 (green) and DAPI (blue). Boxes indicate area shown in the zoom panels. Scale bar
1126 represents 20 μm. (B) Fixed cells were stained for CellProfiler analysis as detailed in the
1127 methods. CellProfiler was used to count nuclei, EDC4 puncta and DDX6 puncta. In RStudio
1128 analysis, puncta with $\geq$ 60% correlation (mean correlation in vector control) between EDC4 and
1129 DDX6 (PBs) were counted and normalized to number of nuclei per condition. PB counts were
1130 normalized to vector control within each replicate.
1131

1132 **Figure 7: YAP Inputs Mediate PB Disassembly.** (A, B) HUVECs were seeded onto collagen-
1133 coated microscope slides and exposed to shear stress of 2 dyn/cm^2, 10 dyn/cm^2 or no shear (static
1134 control) for 21 h. Cells were fixed and stained for immunofluorescence. (A) Representative
1135 images of cells stained for PB-resident proteins EDC4 (green) and DDX6 (blue), as well as F-
1136 actin (red, phalloidin). Boxes indicate area shown in EDC4 (zoom) and DDX6 (zoom) panels.
1137 Scale bar represents 20 μm. (B) CellProfiler was used to count nuclei, EDC4 puncta and DDX6
1138 puncta. In RStudio analysis, puncta with $\geq$ 70% correlation (mean correlation in vector control)
1139 between EDC4 and DDX6 (PBs) were counted and normalized to number of nuclei per
1140 condition. PB counts were normalized to static control within each replicate. (C, D) HUVECs
1141 were split and seeded at a high-, medium- and low-density, cultured for 48 h and fixed for
1142 immunofluorescence. (C) Representative images of cells stained for the PB-resident protein
1143 EDC4 (green) and F-actin (red, phalloidin). Boxes indicate images shown in EDC4 (zoom)
1144 panel. Scale bar represents 20 μm. (D) Fixed cells were stained for CellProfiler analysis as
1145 detailed in the methods. The number of EDC4 puncta per cell was quantified and normalized to
1146 the high confluence condition. (E, F) Coverslips were coated for 4 h with 0 to 64 μg/cm^2 of
1147 collagen. HUVECs were grown for 72 h on coated coverslips and fixed for immunofluorescence.
1148 (E) Representative images of cells stained for PB-resident protein EDC4 (green), DDX6 (blue)
1149 and F-actin (red, phalloidin). Boxes indicate images shown in EDC4 (zoom) panel. Scale bar
1150 represents 20 μm. (F) Fixed cells were stained for CellProfiler analysis as detailed in the
1151 methods. The number of EDC4 puncta per cell was quantified and normalized to the 0 μg/mL
1152 collagen-coating condition. Statistics were determined using repeated measures ANOVA (A, B)
1153 or Pearson's correlation co-efficient (C); error bars represent standard deviation (A, B) and 95%
1154 confidence interval of line of best fit (slope is significantly non-zero, $p = 0.014$) (C); n=3
1155 independent biological replicates; * = $p < 0.05$, ** = $p < 0.01$.
1156
1157 **Figure 8: YAP is required for EDC4 puncta disassembly in HUVECs subjected to shear**
1158 **stress.** (A) HUVECs were seeded onto collagen-coated microscope slides and exposed to shear
1159 stress of 2 dyn/cm^2, 10 dyn/cm^2 or a static control for 21 h. Cells were lysed for immunoblotting.
1160 One representative immunoblot and quantification of three independent experiments stained with
1161 P(S127)-YAP- and YAP-specific antibody is shown. P(S127)-YAP and YAP protein levels in
1162 each condition were normalized to total protein. All treatments were normalized to static control

1163 within each replicate. (B, C) HUVECs were transduced with shRNAs targeting YAP (shYAP-2)
1164 or with a non-targeting (shNT) control and selected. Cells were seeded onto collagen-coated
1165 microscope slides and exposed to shear stress of 10 dyn/cm^2 or no shear (static control) for 21 h.
1166 Cells were fixed and stained for immunofluorescence. (B) CellProfiler was used to count nuclei
1167 and EDC4 puncta. In RStudio analysis, EDC4 puncta were normalized to number of nuclei per
1168 condition. EDC4 puncta counts were normalized to static control. (C) Representative images of
1169 cells stained for PB-resident protein EDC4 (red), DDX6 (green) and DAPI (blue). In parallel,
1170 separate coverslips were stained for F-actin (phalloidin). Boxes indicate area shown in the EDC4
1171 (zoom) panel. Scale bar represents 20 μm. Statistics were determined using repeated measures
1172 ANOVA (A); error bars represent standard deviation (A) ; n=4, except 2 dyn/cm^2 (n=3) (A) and
1173 n = 2 (B, C) independent biological replicates; * = $p < 0.05$, ** = $p < 0.01$. (D) KapB activates a
1174 mechanoresponsive pathway from within the cell rather than without to mediate PB disassembly.
1175 Cells respond to external mechanical force by activating their structural support network, the
1176 actin cytoskeleton. The GTPase RhoA and its downstream effectors coordinate this response,
1177 bundling actin filaments into stress fibers (SFs), enhancing actomyosin contractility and
1178 increasing adhesion to the underlying matrix to help withstand force-induced membrane
1179 deformation. Together, these actin-based responses increase cytoskeletal tension and elicit the
1180 dephosphorylation and nuclear translocation of the mechanoresponsive transcription activator
1181 YAP where it collaborates with other transcription factors to induce TEAD-responsive genes.
1182 We present data to support the existence of a mechanoresponsive pathway that links actin SFs,
1183 actomyosin contractility, and the transcription transactivator YAP to the disassembly of PBs.
1184 The viral protein KapB taps into this mechanoresponsive pathway, triggering mechanical
1185 changes and forming contractile cytoskeletal structures that would normally respond to force,
1186 thereby inducing PB disassembly in a YAP-dependent manner, from within the cell, rather than
1187 from without. Both KapB and stimuli that activate YAP cause PB disassembly.
1188
1189 **Figure S1: The RhoA-effector ROCK is required for KapB-mediated PB disassembly,**
1190 **knockdown confirmation and vector data.** (A) KapB- and vector- expressing HUVECs were
1191 treated with 10 μM Y-27632 or water control for 4 h and fixed for immunofluorescence. Fixed
1192 cells were stained for CellProfiler analysis as detailed in the methods. The number of EDC4
1193 puncta per cell was quantified and normalized to the vector control. Vector control data is

1194 shown. (B, C) KapB- and vector- expressing HUVECs were transduced with shRNAs targeting
1195 ROCK1 and ROCK2 (shROCK1-1, shROCK1-2, shROCK2-1, shROCK2-2) or with a non-
1196 targeting (shNT) control and selected. In parallel, cells were lysed for immunoblotting or fixed
1197 for immunofluorescence. (B) One representative immunoblot of three independent experiments
1198 stained using ROCK1- and 2-specific antibodies. (C) Fixed cells were stained for CellProfiler
1199 analysis as detailed in the methods. The number of EDC4 puncta per cell was quantified and
1200 normalized to the vector NT control within each replicate. Vector control data is shown.
1201 Statistics were determined using a ratio paired t-test between control and experimental groups;
1202 error bars represent standard deviation; n=3 independent biological replicates; * = $p < 0.05$.
1203
1204 **Figure S2: Cofilin knockdown augments KapB-mediated PB disassembly.** KapB- and
1205 vector- expressing HUVECs were transduced with shRNAs targeting cofilin (shCFN-1, shCFN-
1206 2) or with a non-targeting (shNT) control and selected. In parallel, cells were fixed for
1207 immunofluorescence or lysed for immunoblotting. (A) One representative immunoblot of three
1208 independent experiments stained using a cofilin-specific antibody. (B, C) Fixed cells were
1209 stained for CellProfiler analysis as detailed in the methods. (B) The number of EDC4 puncta per
1210 cell was quantified and normalized to the vector NT control within each replicate. (C)
1211 CellProfiler data was used to calculate the ratio of EDC4 puncta counts in KapB-expressing cells
1212 versus the vector control for each treatment condition. (D) Representative images of cells stained
1213 for PB-resident protein EDC4 (green), KapB (blue), and F-actin (red, phalloidin). Boxes indicate
1214 the area of the field of view that is shown in EDC4 (zoom) panel. Scale bar represents 20 μm.
1215 Statistics were determined using a ratio paired t-test between control and experimental groups;
1216 error bars represent standard deviation; n=3 independent biological replicates; * = $p < 0.05$.
1217
1218 **Figure S3: KapB does not activate canonical functions of YAP.** (A, B) KapB- and vector-
1219 expressing HUVECs were lysed for immunoblotting or fixed for immunofluorescence. (A)
1220 Representative immunoblots and quantification of immunoblotting for P(S127)-YAP-, YAP- or
1221 KapB-specific antibody are shown. Several immunoblots are shown to illustrate variation in
1222 KapB-mediated changes in P-YAP and YAP. Protein levels in each condition were normalized to
1223 total protein. All treatments were normalized to vector control within each replicate. (B)
1224 Representative images of cells stained for YAP. Scale bar represents 20 μM. (C) HUVECs were

1225 transduced with recombinant lentiviruses expressing KapB, a constitutively active version of
1226 YAP (YAP 5SA) or an empty vector control, selected and lysed for total RNA. qRT-PCR
1227 analysis of steady state mRNA levels of canonical YAP-regulated genes CTGF, ANKRD1 and
1228 CYR61 was performed, and was normalized to steady state HPRT-1 mRNA levels. Statistics
1229 were determined using repeated measures ANOVA; error bars represent standard deviation; n=3
1230 independent biological replicates; * = $p < 0.05$, ** = $p < 0.01$.
1231
1232
1233

1234 **Supplementary Files**

1235 **Table 1:** Table detailing antibodies used in this study, including species, target, source, use and
1236 dilution.

1237

1238 **Table 2:** Table detailing plasmids used in this study, including name, use, source, bacterial
1239 selection cassette and mammalian selection cassette.

1240

1241 **Table 3:** Table detailing shRNA sequences used in this study.

1242

1243 **Table 4:** Table detailing drug treatments used in this study, including name, use, source,
1244 concentration and duration of treatment.

1245

1246 **Table 5:** Table detailing qRT-PCR primers used in this study, including target, sequence,
1247 melting temperature, and reference.

1248

1249 **Source Code**

1250 **Source Code 1**: CellProfiler pipeline used to enumerate puncta from epifluorescent microscopy
1251 images of HUVECs stained for Hedls puncta; co-stained with DAPI and WGA.

1252

1253 **Source Code 2**: CellProfiler pipeline used to enumerate puncta from confocal microscopy
1254 images of HUVECs subjected to shear stress stained for Hedls and DDX6 puncta.

1255

1256 **Source Code 3**: CellProfiler pipeline used to enumerate puncta from confocal microscopy
1257 images of HUVECs subjected to shear stress stained for Hedls puncta.

1258

1259 **Source Code 4**: CellProfiler pipeline used to quantify intensity in nucleus and cytoplasm from
1260 epifluorescent microscopy images of HUVECs stained for YAP protein; co-stained with DAPI
1261 and WGA.

1262

1263 **Source Code 5:** Template RStudio code used for analysis of CellProfiler output from Source
1264 Code 1. Annotations provided within code.

Source Code 6: Template RStudio code used for analysis of CellProfiler output from Source Code 2. Annotations provided within code.

Source Code 7: Template RStudio code used for analysis of CellProfiler output from Source Code 3. Annotations provided within code.

Source Code 8: Template RStudio code used for analysis of CellProfiler output from Source Code 4. Annotations provided within code.

Figure 1

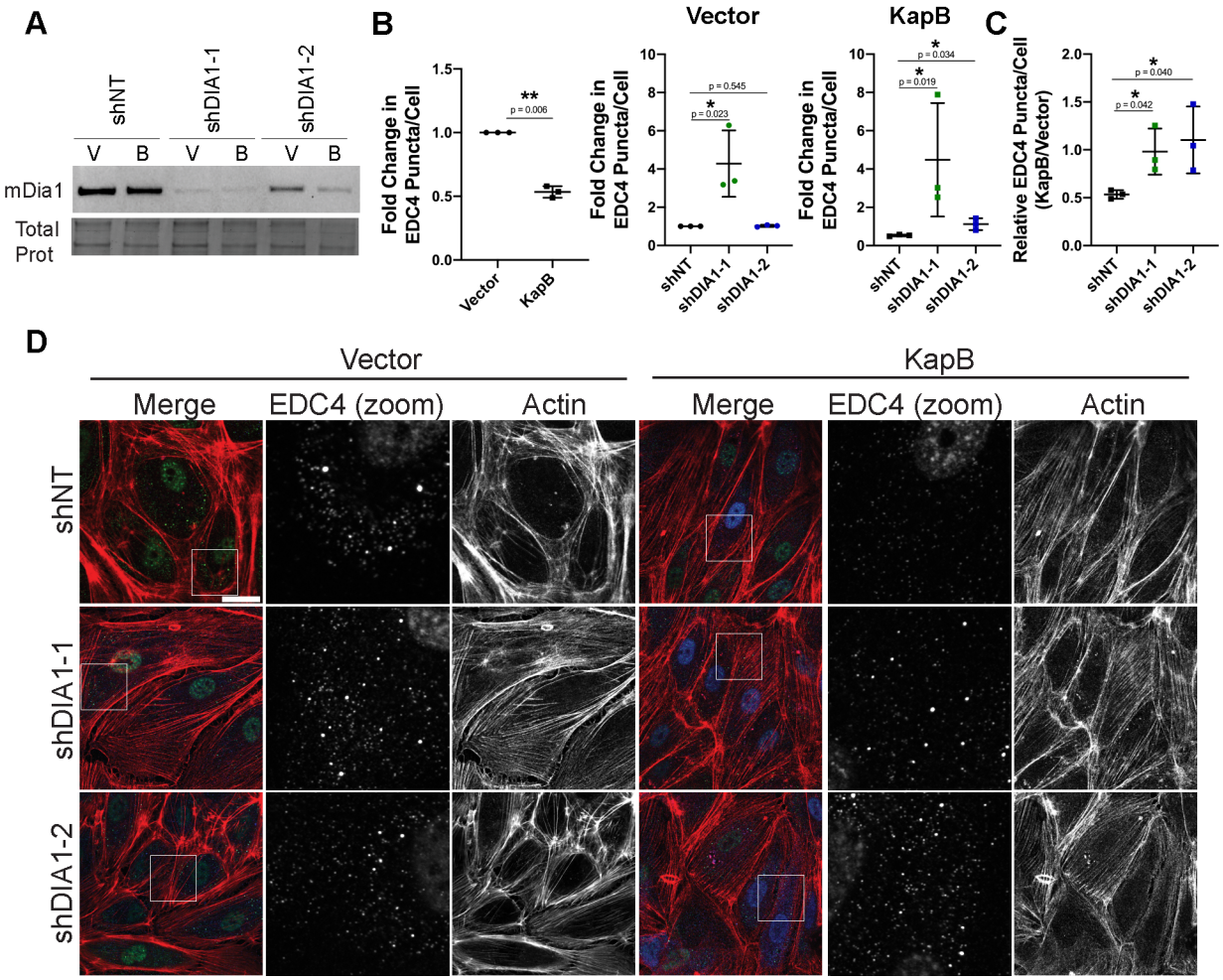
A
shNT
shDIA1-1
shDIA1-2
V B V B V B
mDia1
Total Prot
B
Vector
KapB
Fold Change in EDC4 Puncta/Cell
p = 0.006
p = 0.023
p = 0.545
p = 0.019
p = 0.034
Vector
KapB
shNT
shDIA1-1
shDIA1-2
C
Relative EDC4 Puncta/Cell (KapB/Vector)
p = 0.042
p = 0.040
D
Vector
KapB
Merge
EDC4 (zoom)
Actin
shNT
shDIA1-1
shDIA1-2

Figure 2

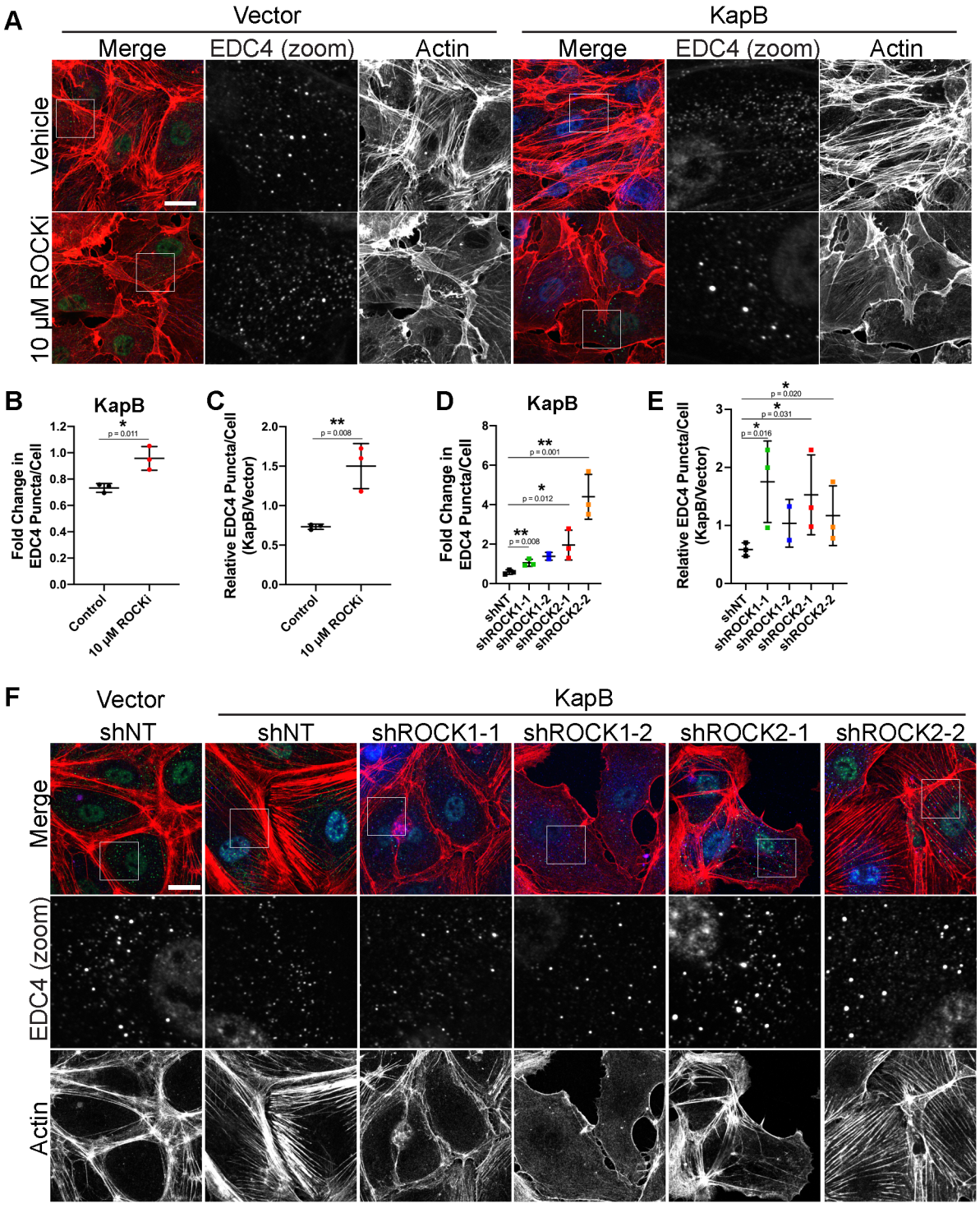
A
Vector
KapB
Merge
EDC4 (zoom)
Actin
Vehicle
10 μM ROCKi
B
KapB
Fold Change in EDC4 Puncta/Cell
p = 0.011
Control
10 μM ROCKi
C
Relative EDC4 Puncta/Cell (KapB/Vector)
p = 0.008
D
KapB
Fold Change in EDC4 Puncta/Cell
p = 0.001
p = 0.012
p = 0.008
shNT
shROCK1-1
shROCK1-2
shROCK2-1
shROCK2-2
E
Relative EDC4 Puncta/Cell (KapB/Vector)
p = 0.020
p = 0.031
p = 0.016
F
Vector
shNT
KapB
shNT
shROCK1-1
shROCK1-2
shROCK2-1
shROCK2-2
Merge
EDC4 (zoom)
Actin

Figure 3

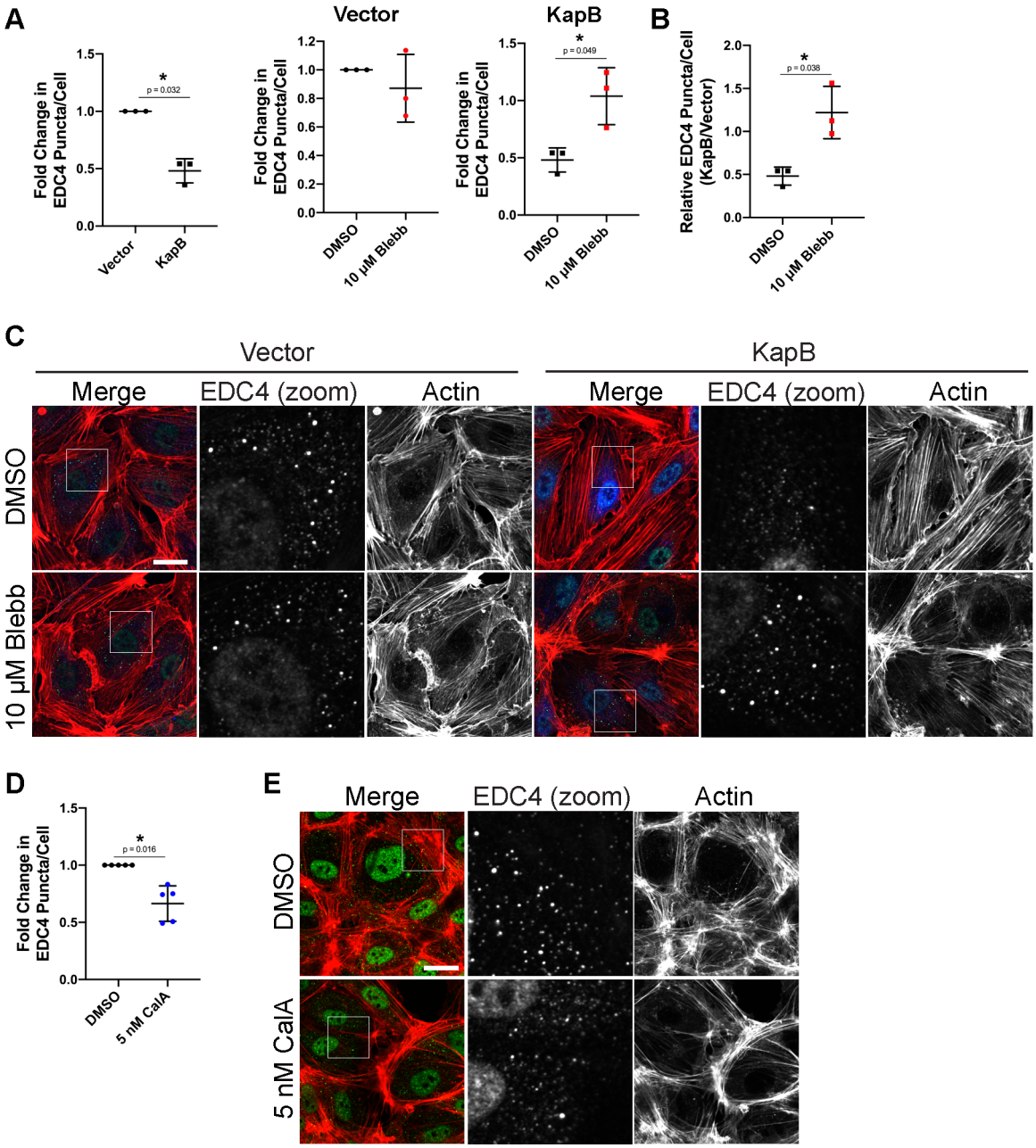
A
Fold Change in EDC4 Puncta/Cell
1.5
1.0
0.5
0.0
*
p = 0.032
Vector
KapB
Vector
Fold Change in EDC4 Puncta/Cell
1.2
1.0
0.8
0.6
0.4
0.2
0.0
DMSO
10 μM Blebb
KapB
Fold Change in EDC4 Puncta/Cell
1.5
1.0
0.5
0.0
*
p = 0.049
DMSO
10 μM Blebb
B
Relative EDC4 Puncta/Cell (KapB/Vector)
2.0
1.5
1.0
0.5
0.0
*
p = 0.038
DMSO
10 μM Blebb
C
Vector
KapB
Merge
EDC4 (zoom)
Actin
Merge
EDC4 (zoom)
Actin
DMSO
10 μM Blebb
D
Fold Change in EDC4 Puncta/Cell
1.5
1.0
0.5
0.0
*
p = 0.016
DMSO
5 nM CalA
E
Merge
EDC4 (zoom)
Actin
DMSO
5 nM CalA

Figure 4

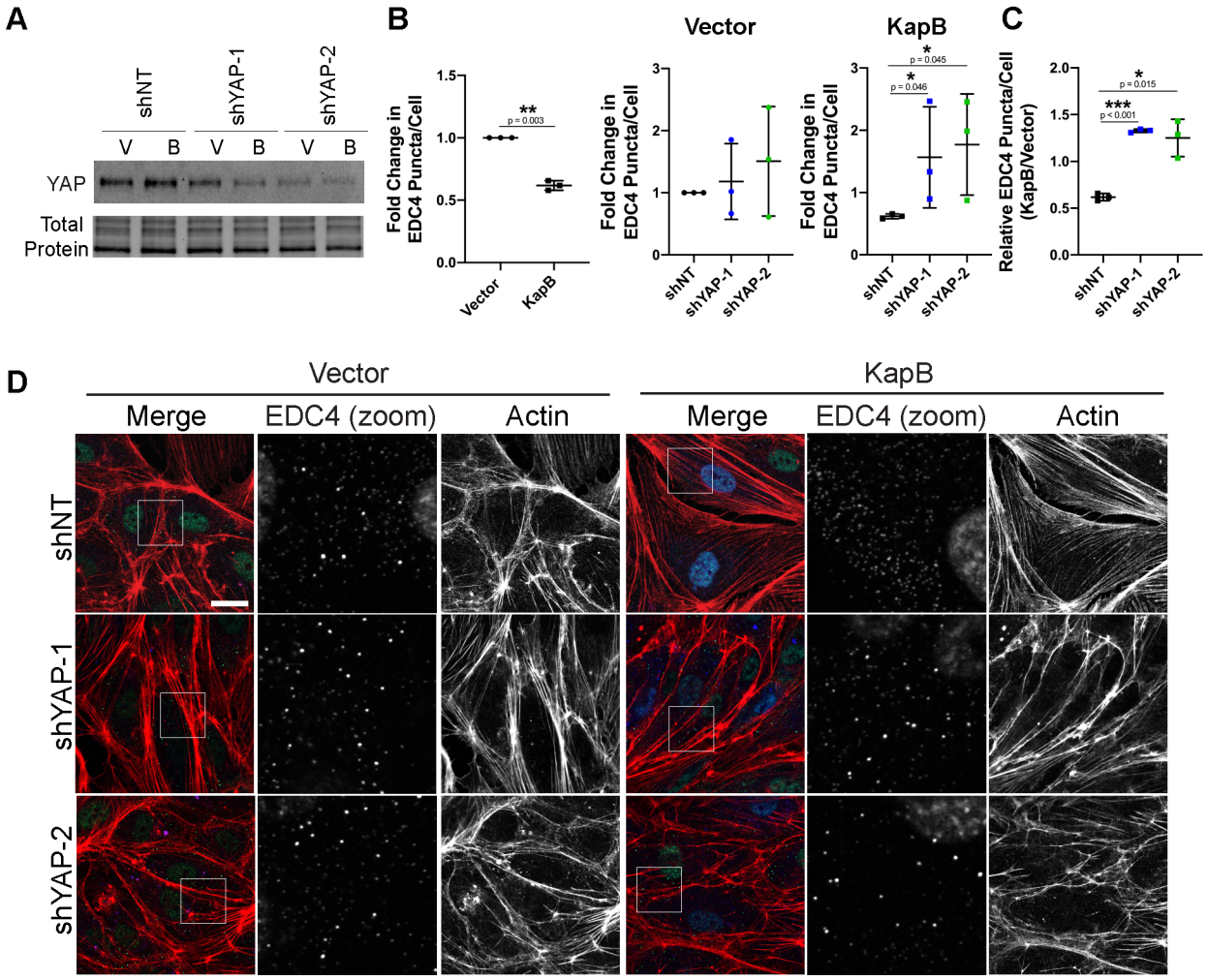
A
shNT
shYAP-1
shYAP-2
V B V B V B
YAP
Total Protein
B
Fold Change in EDC4 Puncta/Cell
**
p = 0.003
Vector
KapB
Vector
KapB
*
p = 0.045
*
p = 0.046
shNT
shYAP-1
shYAP-2
C
Relative EDC4 Puncta/Cell (KapB/Vector)
*
p = 0.015
***
p < 0.001
D
Vector
KapB
Merge
EDC4 (zoom)
Actin
shNT
shYAP-1
shYAP-2

Figure 5

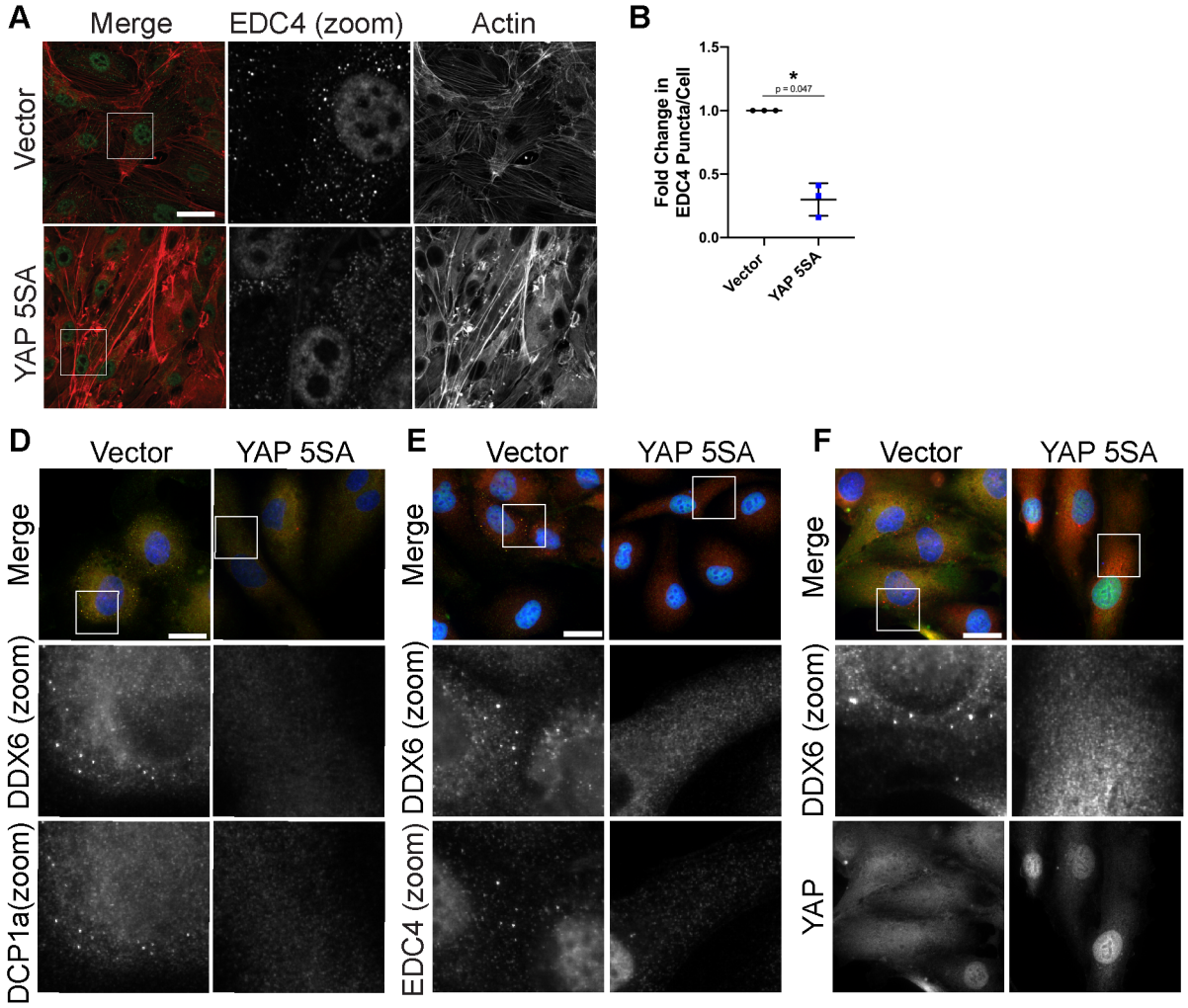
A
Merge
EDC4 (zoom)
Actin
Vector
YAP 5SA
B
Fold Change in EDC4 Puncta/Cell
1.5
1.0
0.5
0.0
*
p = 0.047
Vector
YAP 5SA
D
Vector
YAP 5SA
Merge
DDX6 (zoom)
DCP1a(zoom)
E
Vector
YAP 5SA
Merge
DDX6 (zoom)
EDC4 (zoom)
F
Vector
YAP 5SA
Merge
DDX6 (zoom)
YAP

Figure 6

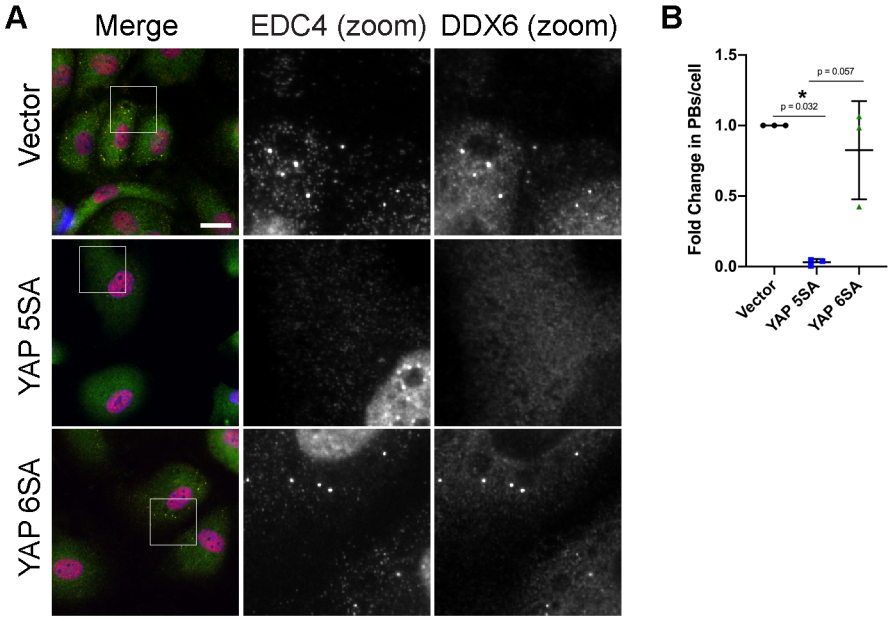
A
Merge
EDC4 (zoom)
DDX6 (zoom)
Vector
YAP 5SA
YAP 6SA
B
Fold Change in PBs/cell
1.5
1.0
0.5
0.0
p = 0.057
*
p = 0.032
Vector
YAP 5SA
YAP 6SA

Figure 7

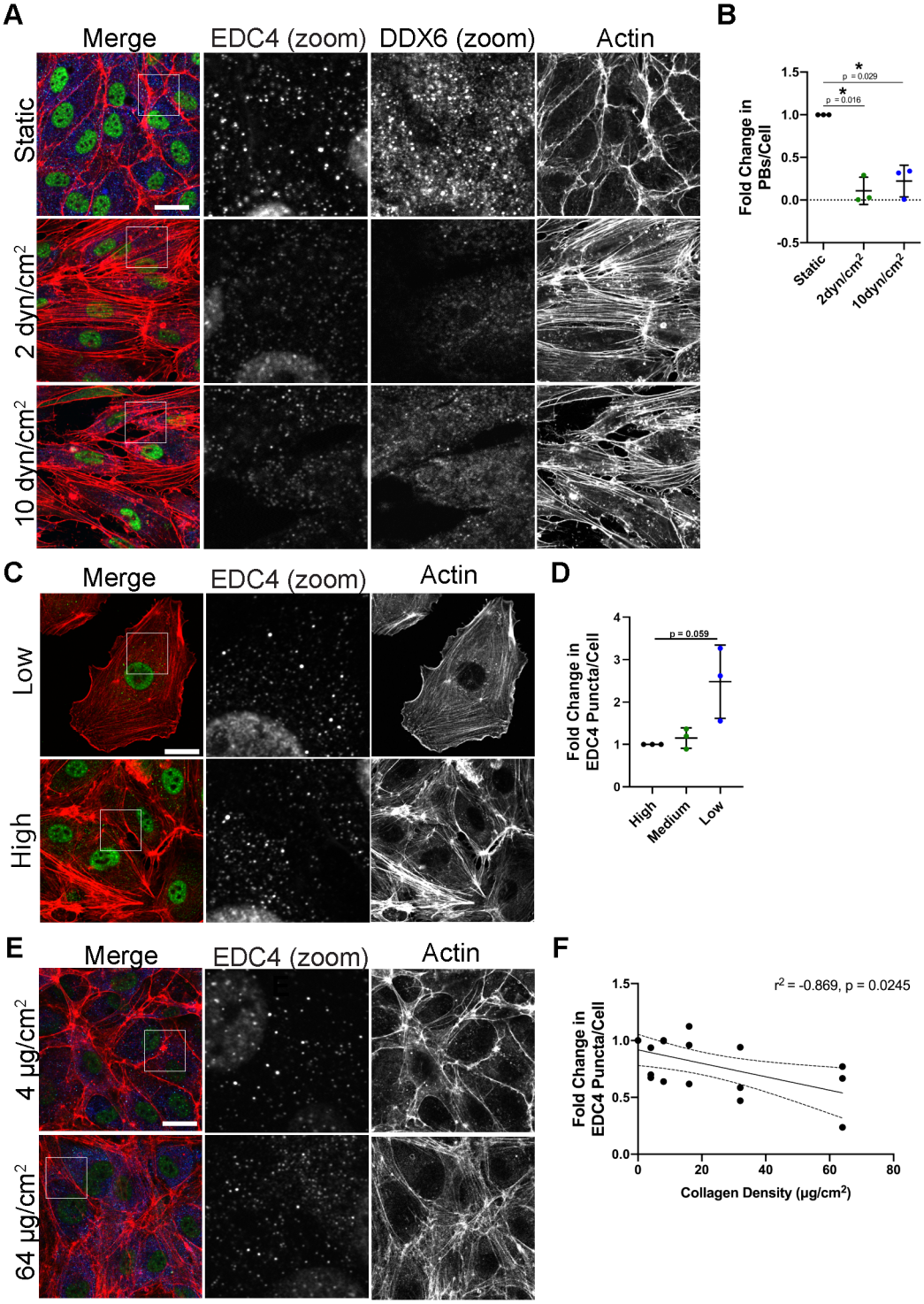
A
Merge
EDC4 (zoom)
DDX6 (zoom)
Actin
Static
2 dyn/cm2
10 dyn/cm2
B
Fold Change in PBs/Cell
p = 0.029
p = 0.016
Static
2dyn/cm2
10dyn/cm2
C
Merge
EDC4 (zoom)
Actin
Low
High
D
Fold Change in EDC4 Puncta/Cell
p = 0.059
High
Medium
Low
E
Merge
EDC4 (zoom)
Actin
4 µg/cm2
64 µg/cm2
F
r2 = -0.869, p = 0.0245
Fold Change in EDC4 Puncta/Cell
Collagen Density (µg/cm2)

Figure 8

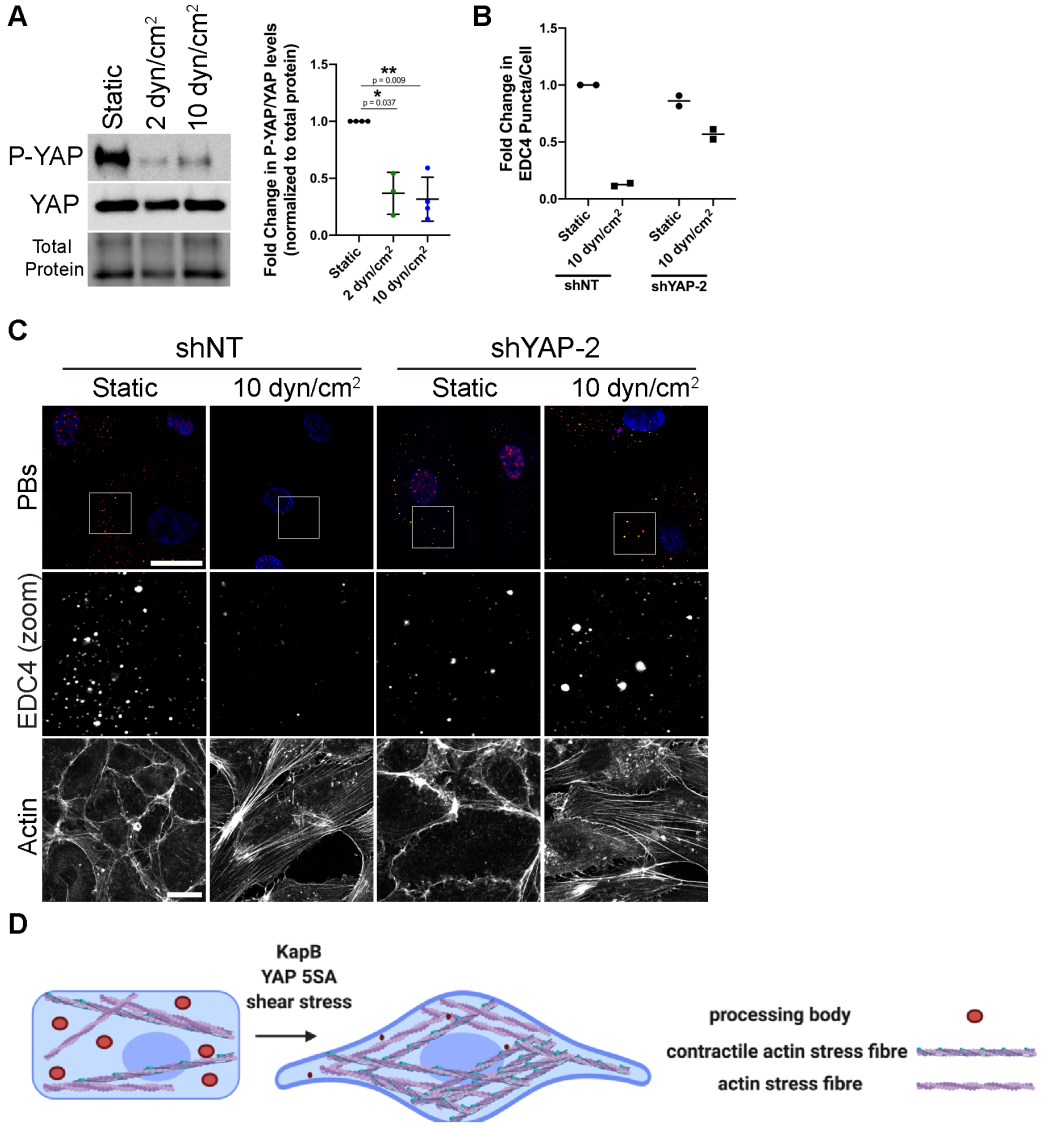
A
Static
2 dyn/cm2
10 dyn/cm2
P-YAP
YAP
Total Protein
Fold Change in P-YAP/YAP levels (normalized to total protein)
1.5
1.0
0.5
0.0
**
p = 0.009
*
p = 0.037
Static
2 dyn/cm2
10 dyn/cm2
B
Fold Change in EDC4 Puncta/Cell
1.5
1.0
0.5
0.0
Static
10 dyn/cm2
Static
10 dyn/cm2
shNT
shYAP-2
C
shNT
shYAP-2
Static
10 dyn/cm2
Static
10 dyn/cm2
PBs
EDC4 (zoom)
Actin
D
KapB
YAP 5SA
shear stress
processing body
contractile actin stress fibre
actin stress fibre

Figure S1

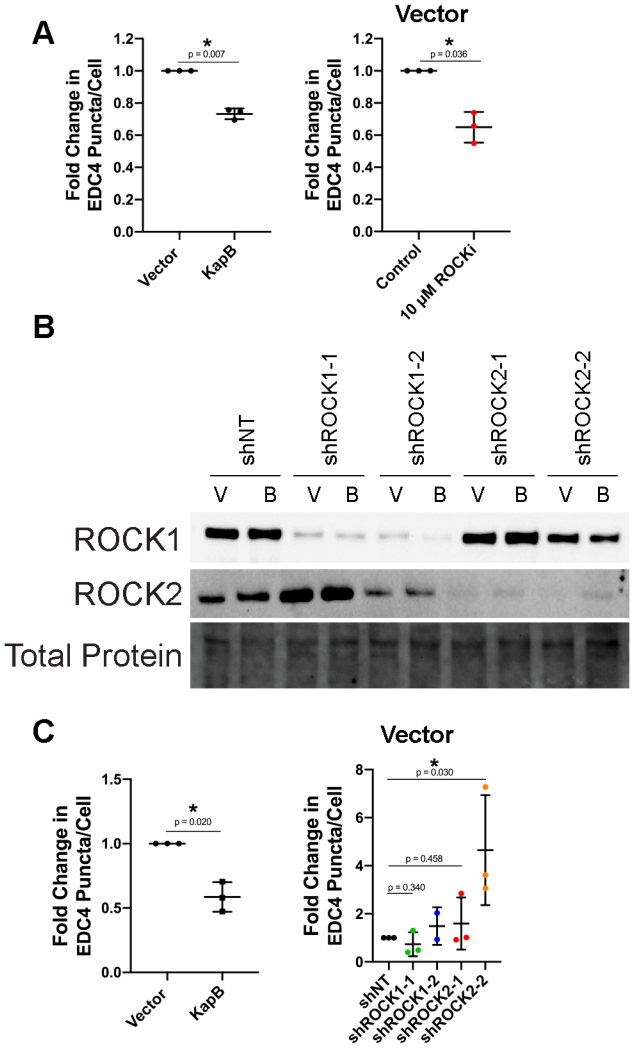
A
Vector
Fold Change in EDC4 Puncta/Cell
p = 0.007
Vector
KapB
p = 0.036
Control
10 μM ROCKi
B
shNT
shROCK1-1
shROCK1-2
shROCK2-1
shROCK2-2
V B V B V B V B V B
ROCK1
ROCK2
Total Protein
C
Vector
Fold Change in EDC4 Puncta/Cell
p = 0.020
Vector
KapB
p = 0.030
p = 0.458
p = 0.340
shNT
shROCK1-1
shROCK1-2
shROCK2-1
shROCK2-2

Figure S2

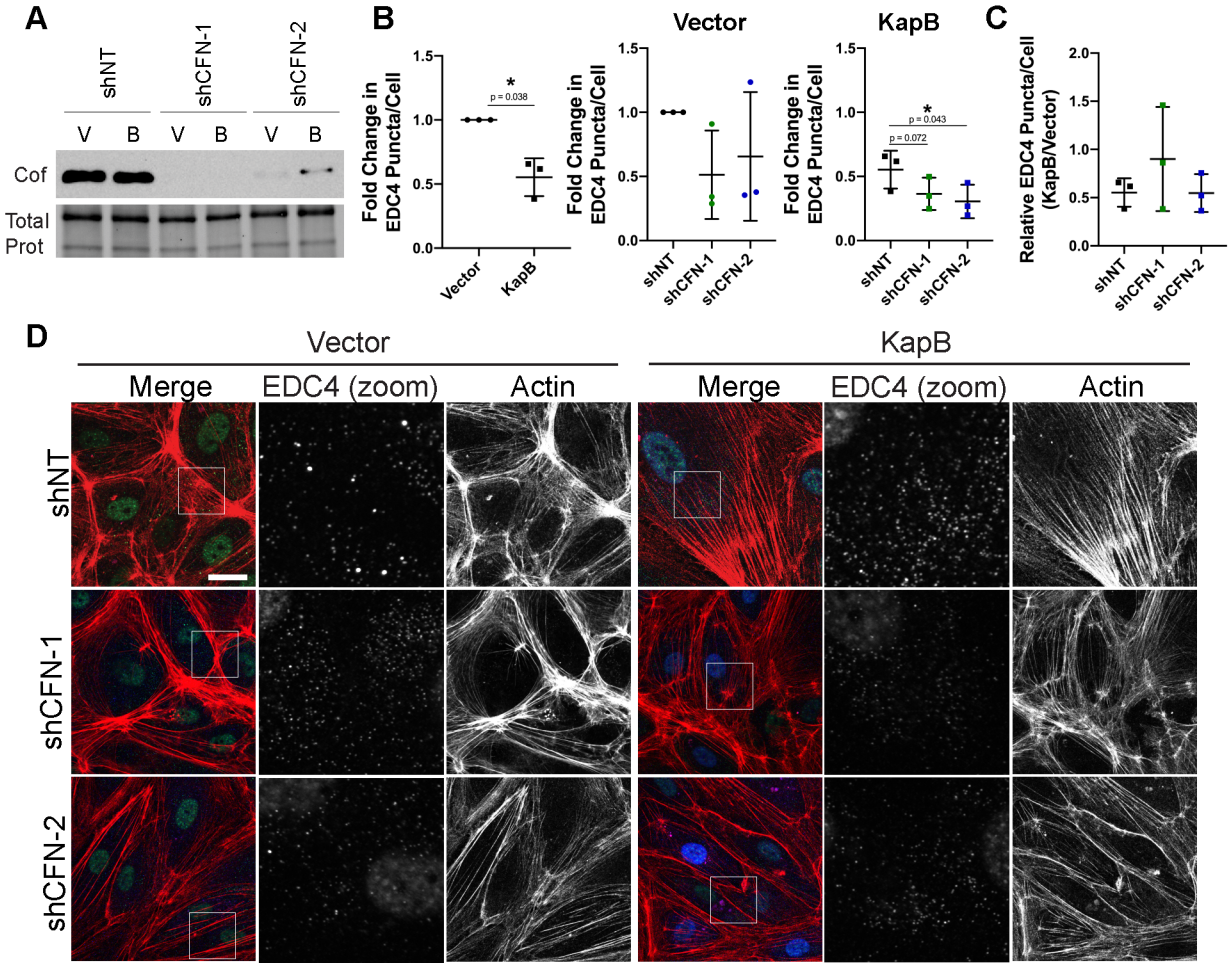
A
shNT
shCFN-1
shCFN-2
V B V B V B
Cof
Total Prot
B
Fold Change in EDC4 Puncta/Cell
p = 0.038
Vector
KapB
Vector
KapB
p = 0.043
p = 0.072
shNT
shCFN-1
shCFN-2
C
Relative EDC4 Puncta/Cell (KapB/Vector)
D
Vector
KapB
Merge
EDC4 (zoom)
Actin
shNT
shCFN-1
shCFN-2

Figure S3

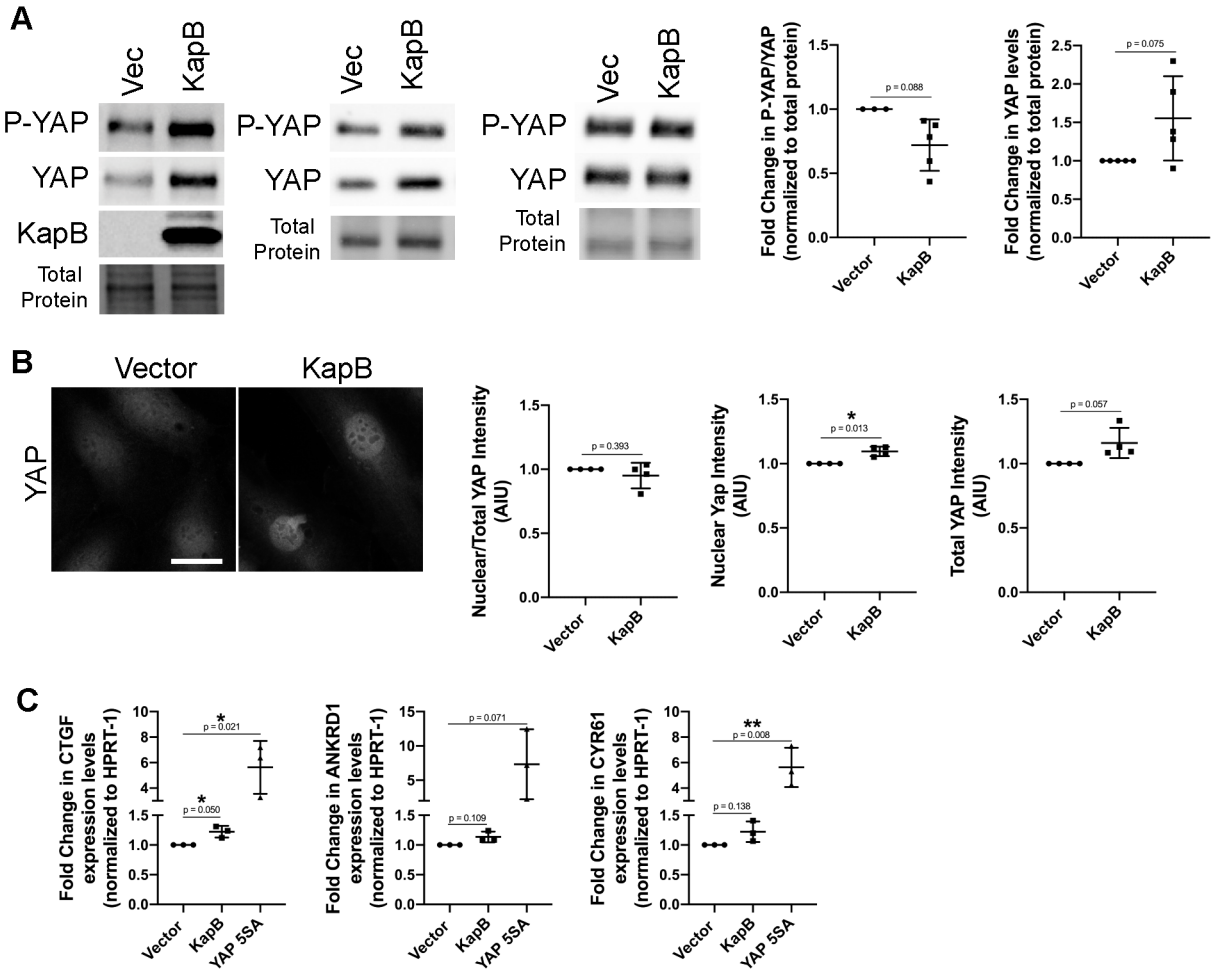
A
Vec
KapB
P-YAP
YAP
KapB
Total Protein
Vec
KapB
P-YAP
YAP
Total Protein
Vec
KapB
P-YAP
YAP
Total Protein
Fold Change in P-YAP/YAP (normalized to total protein)
p = 0.088
Vector
KapB
Fold Change in YAP levels (normalized to total protein)
p = 0.075
Vector
KapB
B
Vector
KapB
YAP
Nuclear/Total YAP Intensity (AIU)
p = 0.393
Vector
KapB
Nuclear Yap Intensity (AIU)
*
p = 0.013
Vector
KapB
Total YAP Intensity (AIU)
p = 0.057
Vector
KapB
C
Fold Change in CTGF expression levels (normalized to HPRT-1)
*
p = 0.021
*
p = 0.050
Vector
KapB
YAP 5SA
Fold Change in ANKRD1 expression levels (normalized to HPRT-1)
p = 0.071
p = 0.109
Vector
KapB
YAP 5SA
Fold Change in CYR61 expression levels (normalized to HPRT-1)
**
p = 0.008
p = 0.138
Vector
KapB
YAP 5SA

Supplementary Table 1: Antibodies used in this study.

Antibody	Source	Use	Dilution
Rabbit α-mDia1	Cell Signalling Technologies (Cat#:5486)	Immunoblotting	1:1000 in 2.5% BSA
Rabbit α-ROCK1	Cell Signalling Technologies (Cat#:4035)	Immunoblotting	1:1000 in 2.5% BSA
Rabbit α-ROCK2	Cell Signalling Technologies (Cat#:9029)	Immunoblotting	1:500 in 2.5% BSA
Rabbit α-Cofilin	Cell Signalling Technologies (Cat#:5175)	Immunoblotting	1:1000 in 2.5% BSA
Rabbit α-P-YAP	Cell Signalling Technologies (Cat#: 4911)	Immunoblotting	1:1000 in 2.5% BSA
Rabbit α-YAP	Cell Signalling Technologies (Cat#: 4912)	Immunoblotting	1:1000 in 2.5% BSA
α-Mouse IgG, HRP-linked (2˚)	Cell Signalling Technologies (Cat#: 7076)	Immunoblotting	1:2000 to 1:4000 in 2.5% BSA
α-Rabbit IgG, HRP-linked (2˚)	Cell Signalling Technologies (Cat#: 7074)	Immunoblotting	1:2000 to 1:4000 in 2.5% BSA

Mouse α-p70 s6 kinase (detects EDC4)	Santa Cruz (Cat#:sc-8418)	Immunofluorescence	1:1000 in blocking buffer (1% Human AB in PBS), 4˚C overnight
Rabbit α-KapB	Gift from D. Ganem and C. McCormick	Immunofluorescence/ Immunoblotting	1:1000 in blocking buffer (1% Human AB in PBS), 30 min RT
Mouse α-YAP	Santa Cruz (Cat#:sc-101199)	Immunofluorescence	1:1000 in blocking buffer (1% Human AB in PBS), 4˚C overnight
Rabbit α-DDX6	Bethyl Labs (Cat#:A300-461A)	Immunofluorescence	1:1000 in blocking buffer (1% Human AB in PBS), 4˚C overnight
Rabbit α-β-actin HRP-linked	Cell Signalling Technologies (Cat #:5125)	Immunoblotting	1:2000 in 2.5% BSA
Alexa Fluor 555-conjugated donkey α-mouse IgG (2˚)	Invitrogen (Cat#:A31570)	Immunofluorescence	1:1000 in blocking buffer (1% Human AB in PBS), 1h RT
Alexa Fluor 488-conjugated chicken α-rabbit IgG (2˚)	Invitrogen (Cat#:A21441)	Immunofluorescence	1:1000 in blocking buffer (1% Human AB in PBS), 1h RT
Alexa Fluor 555-conjugated donkey α-rabbit IgG (2˚)	Invitrogen (Cat#:A31572)	Immunofluorescence	1:1000 in blocking buffer (1% Human AB in PBS), 1h RT
Alexa Fluor 488-conjugated chicken α-mouse IgG (2˚)	Invitrogen (Cat#:A21200)	Immunofluorescence	1:1000 in blocking buffer (1% Human AB in PBS), 1h RT

Supplementary Table 2: Plasmids used in this study.

Plasmid Name	Use	Source	Bacterial Selection Cassette	Mammalian Selection Cassette (Lentiviral Plasmids Only)
pLJM-1-EV	Control vector for lentiviral expression studies	C. McCormick (Dalhousie University)	Ampicillin	Blasticidin, Puromycin
pLJM-1 KapB	Lentiviral expression of KapB	C. McCormick (Dalhousie University)	Ampicillin	Blasticidin
pLKO-(shRNA)	Lentiviral expression of short hairpin RNAs (shRNA sequences in Table S3)	Cloned from: pLKO-TRC Addgene no.: 26655	Ampicillin	Puromycin
pLJM-1-YAP-5SA (CA-YAP)	Lentiviral expression of constitutively active YAP	Cloned from: p2XFLAG-YAP-5SA, Donated by C. McCormick (Dalhousie University)	Ampicillin	Blasticidin
pcDNA3.1	Transfection control	Invitrogen	Ampicillin	N/A
pcDNA3.1 KapB	Transfection of KapB	C. McCormick (Dalhousie University)	Ampicillin	N/A
p1XFLAG	Transfection control	Cloned from: p2XFLAG-YAP-5SA, Donated by C. McCormick (Dalhousie University)	Ampicillin	N/A

p2XFLAG-YAP 5SA	Transfection of YAP 5SA	Donated by C. McCormick (Dalhousie University)	Ampicillin	N/A
pV5-YAP 6SA	Transfection of YAP 6SA	Addgene no: 42562	Ampicillin	N/A
pMD2.G	Envelope protein for lentiviral production	Addgene no: 12259	Ampicillin	N/A
psPAX2	Packaging proteins for lentiviral production	Addgene no: 12260	Ampicillin	N/A

Supplementary Table 3: shRNA sequences used in this study.

Target	Sequence (5' – 3')
Non-targeting sense	CCGGAGCACAAGCTGGAGTACAACTACTCGAGATCAACATGAGGTCGAACACGATTTG
Non-targeting antisense	AATTCAAAAAGCACAAGCTGGAGTACAACTAATCAACATGAGGTCGAACACGATTTG
mDia1 sh1 sense	CCGGCCAATTCTGCTCATAGAAATTCTCGAGAATTTCTATGAGCAGAATTGGTTTTTG
mDia1 sh1 antisense	AATTCAAAAACCAATTCTGCTCATAGAAATTCTCGAGAATTTCTATGAGCAGAATTGG
mDia1 sh2 sense	CCGGAAGATGACGTTGTTACACTTCCTCGAGGAAGTGTAACAACGTCATCTTTTTTTG
mDia1 sh2 antisense	AATTCAAAAAAAGATGACGTTGTTACACTTCCTCGAGGAAGTGTAACAACGTCATCTT
ROCK1 sh1 sense	CCGGAAGATGACGTTGTTACACTTCCTCGAGGAAGTGTAACAACGTCATCTTTTTTTG
ROCK1 sh1 antisense	AATTCAAAAAAAGATGACGTTGTTACACTTCCTCGAGGAAGTGTAACAACGTCATCTT
ROCK1 sh2 sense	CCGGAAGATGACGTTGTTACACTTCCTCGAGGAAGTGTAACAACGTCATCTTTTTTTG
ROCK1 sh2 antisense	AATTCAAAAAAAGATGACGTTGTTACACTTCCTCGAGGAAGTGTAACAACGTCATCTT
ROCK2 sh1 sense	CCGGCGTTGCCATATTAAGTGTCATCTCGAGATGACACTTAATATGGCAACGTTTTTG
ROCK2 sh1 antisense	AATTCAAAAACGTTGCCATATTAAGTGTCATCTCGAGATGACACTTAATATGGCAACG
ROCK2 sh2 sense	CCGGGCCTTGCATATTGGTCTGGATCTCGAGATCCAGACCAATATGCAAGGCTTTTTG
ROCK2 sh2 antisense	AATTCAAAAAGCCTTGCATATTGGTCTGGATCTCGAGATCCAGACCAATATGCAAGGC

Cofilin sh1 sense	CCGGACGACATGAAGGTGCGTAAGTCTCGAGACTTACGCACCTTCATGTCGTTTTTTG
Cofilin sh1 antisense	AATTCAAAAAACGACATGAAGGTGCGTAAGTCTCGAGACTTACGCACCTTCATGTCGT
Cofilin sh2 sense	CCGGCCAGATAAGGACTGCCGCTATCTCGAGATAGCGGCAGTCCTTATCTGGTTTTTG
Cofilin sh2 antisense	AATTCAAAAACCAGATAAGGACTGCCGCTATCTCGAGATAGCGGCAGTCCTTATCTGG
YAP sh1 sense	CCGGCTGGTCAGAGATACTTCTTAACTCGAGTTAAGAAGTATCTCTGACCAGTTTTTC
YAP sh1 antisense	AATTGAAAAACTGGTCAGAGATACTTCTTAACTCGAGTTAAGAAGTATCTCTGACCAG
YAP sh2 sense	CCGGAAGCTTTGAGTTCTGACATCCCTCGAGGGATGTCAGAACTCAAAGCTTTTTTTC
YAP sh2 antisense	AATTGAAAAAAAGCTTTGAGTTCTGACATCCCTCGAGGGATGTCAGAACTCAAAGCTT

Supplementary Table 4: Drug treatments used in this study.

Drug	Use	Source (Cat#)	Concentration Used	Duration
Y-27623 dihydrochloride (ROCKi)	Non-isoform specific inhibition of ROCK	Sigma-Aldrich (Cat#:Y0503)	10 μM	4 h
(-)-Blebbistatin	Inhibition of MLC contractility	Sigma-Aldrich (Cat#:B0560)	10 μM	30 min
Calyculin A	Inhibition of MLC phosphatase, resulting in cell contraction	Abcam (Cat#: ab141784)	2.5 nM, 5 nM	20 min

Supplementary Table 5: qRT-PCR primers used in this study.

Target	Forward/ Reverse	Sequence	Tm (˚C)	Reference
CYR61	Forward	ATGGTCCCAGTGCTCAAAGA	60	(K.-C. Wang et al. 2016)
CYR61	Reverse	GGGCCGGTATTTCTTCACAC	62	(K.-C. Wang et al. 2016)
CTGF	Forward	CAGCATGGACGTTCGTCTG	60	(K.-C. Wang et al. 2016)
CTGF	Reverse	AACCACGGTTTGGTCCTTGG	62	(K.-C. Wang et al. 2016)
CTGF	Forward	CCCTCGCGGCTTACCG	56	(K.-C. Wang et al. 2016)
CTGF	Reverse	GGACCAGGCAGTTGGCTCT	62	(K.-C. Wang et al. 2016)
ANKRD1	Forward	ACGCCAAAGACAGAGAAGGA	60	(K.-C. Wang et al. 2016)
ANKRD1	Reverse	TACTGCCAAGGTAGCACAAG	52	(K.-C. Wang et al. 2016)
HPRT-1	Forward	CTTTCCTTGGTCAGGCAGTATAA	66	(Singh, 2019)
HPRT-1	Reverse	AGTCTGGCTTATATCCAACACTTC	60	(Singh, 2019)
HPRT-1	Forward	TGGCGTCGTGATTAGTGATG	64	(Singh, 2019)
HPRT-1	Reverse	GACGTTCAGTCCTGTCCATAAT	68	(Singh, 2019)